Journal of Medicinal Chemistry

pubs.acs.org/jmc

Article

p-Alkoxy-Substituted Anisomycins with Potent Anti-Trypanosomiasis Activity and Expanded Modes of Action

Kajumee Bora Bhowal, Anh Minh Thao Nguyen, Ana Victoria Ibarra-Meneses, Andressa Brito Lira, K. Shanmugha Rajan, Jesus D. Castaño, Francis Beaudry, Anat Bashan, Christopher Fernandez-Prada,* Martin Olivier,* Ada Yonath,* and William D. Lubell*

Cite This: *J. Med. Chem.* 2025, 68, 20264−20282

Read Online

ACCESS | Metrics & More | Article Recommendations | Supporting Information

ABSTRACT: Neglected tropical diseases caused by trypanosomatid parasites present a major public healthcare issue, partly due to emerging resistance. Attachment of ω-alkynyl chains characteristic of the lipid tails of antiparasitic peptides to the *p*-position of anisomycin gave ethers exhibiting potent activity, rivalling that of the parent ribosomal inhibitor, especially against resistant *Leishmania* strains. Single-particle cryoelectron microscopy analysis revealed that *O*-propargyl anisomycin binds to the highly conserved peptidyl transferase center of the ribosome similar to the parent inhibitor. Thermal proteomic profiling and gene ontology analysis demonstrated that *O*-propargyl anisomycin exhibited a broader mode of action, including activity against glycosome-associated proteins. Alkynyl substituents improved antiparasitic activity against resistant strains, likely by enlarging the mode of action, offering a novel path toward therapy against trypanosomatid infections.

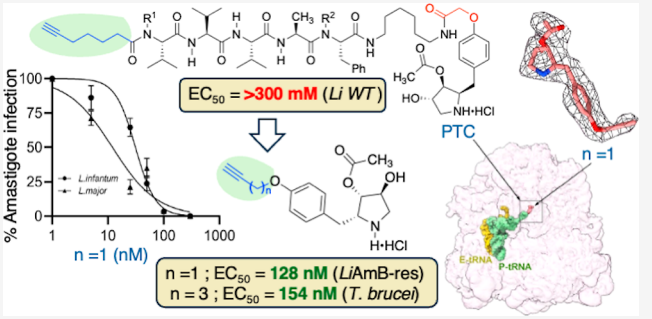

INTRODUCTION

Trypanosomatid parasite neglected tropical diseases (NTDs) pose significant health risks.[1] Leishmaniasis, Human African Trypanosomiasis (HAT), and Chagas disease (CD) collectively affect millions, particularly in tropical and subtropical regions.[2−4] Current therapy has been undermined by parasite resistance, which is exacerbated by urbanization, globalization, and poor healthcare infrastructure.[5,6] Although vaccine development is desired,[7−11] chemotherapy remains the standard of care for treating Trypanosomatid infections.[12] Effective, inexpensive medications are urgently required to surmount inadequacies of current outdated therapeutics to overcome resistant parasite strains without host toxicity.[1,13]

Leishmaniasis is transmitted by the bite of infected female phlebotomine sand flies and occurs primarily in regions of South Asia, the Mediterranean, and South America. The visceral leishmaniasis form, which can lead to hepatosplenomegaly, anemia, and death, is one of the four clinical manifestations, alongside cutaneous, mucocutaneous, and post-kala-azar dermal leishmaniasis.[14] Antileishmanial drugs, such as miltefosine (**1**), sodium stibogluconate (**2**), and amphotericin B (**3**, Figure 1), have limited utility due in part to gene transfer from resistant strains, host toxicity, and restrictive costs.[14]

HAT is caused by *Trypanosoma* (*T.*) *brucei gambiense* and *Trypanosoma brucei rhodesiense*, which are spread by two species of tsetse flies, primarily in West and Central Africa. HAT progresses from the hemolymphatic stage to the fatal encephalitic stage.[15] Despite issues of host toxicity and parasite resistance, older therapies, such as pentamidine (**4**), remain the standard of care for HAT. The causative parasite of CD, *Trypanosoma cruzi*, is transmitted to humans by several species of the triatominae (kissing bug) primarily in Latin America.[16] Often asymptomatic in the acute phase, CD can cause chronic cardiomyopathy and gastrointestinal disorders in 30−40% of infected individuals.[16,17]

In the 21st century, substantial effort has been made to develop new treatments for trypanosomatid infections. Certain chemical entities have entered clinical trials.[18−21] For example, Fexinidazole (**5**) received Food and Drug Administration approval for oral treatment for early stage HAT.[22] Resistance has, however, been reported against the common activation mechanism of such nitroimidazole drugs.[23]

In clinical trials, oral acoziborole (**6**) exhibited efficacy and a favorable safety profile against HAT.[24] For leishmaniasis, pyrrolopyrimidine DNDI-6174 is a preclinical candidate, which targets cytochrome bc1.[25] The nonapeptide Lefleuganan

Received: May 11, 2025
Revised: September 1, 2025
Accepted: September 4, 2025
Published: September 22, 2025

https://doi.org/10.1021/acs.jmedchem.5c01291
J. Med. Chem. 2025, 68, 20264−20282

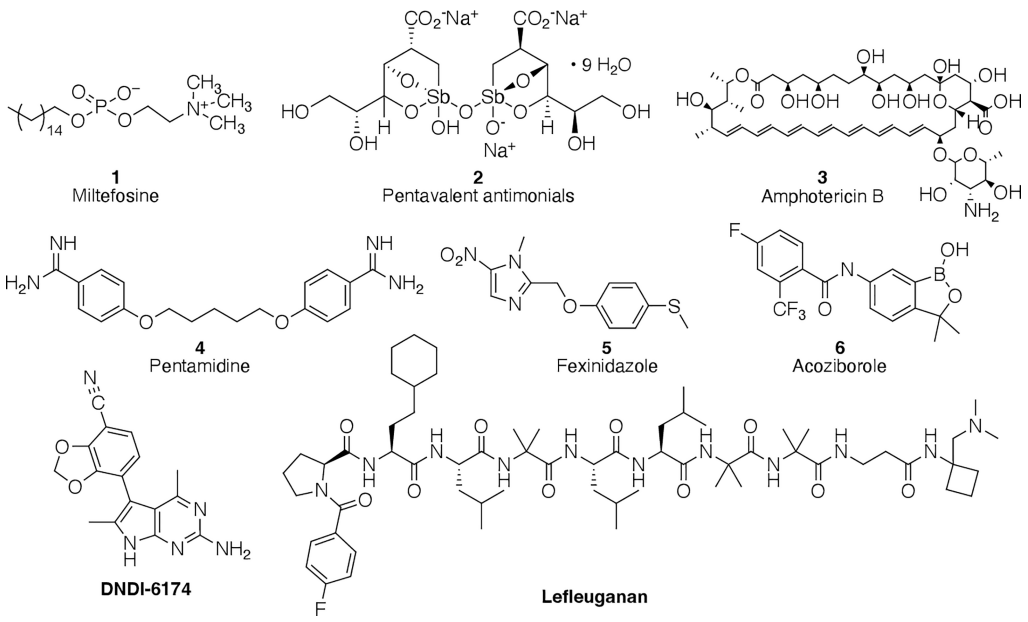

Figure 1. Conventional medications and those in development to treat leishmaniasis and HAT.

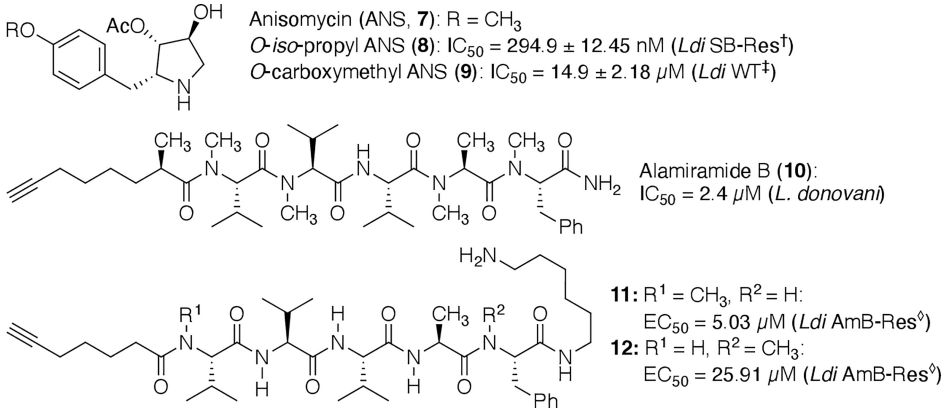

Figure 2. Anisomycin (7), almiramide (**10**),[45] and derivatives **8**, **9**, **11**, and **12**.[44,46] *Leishmania* (*L.*) *infantum* (MHOM/MA/67/ITMAP-263), †resistant to 2 mM trivalent (and pentavalent) antimonials, ‡WT = wild type, ◊resistant to 1 μM amphotericin B.

has shown promise as a clinical candidate that causes membrane disruption.[26]

Despite the potential for drug−drug interactions due to complex pharmacokinetics,[27] interest has shifted toward combination therapy to treat trypanosomatid infection because of resistance and the limited efficacy of monotherapies.[28−30] Single dual-targeting drugs may, however, offer greater potential to avoid drug−drug interactions, improve pharmacological properties, and deliver therapy for administration in a simplified regimen to enhance patient compliance.[27,31] Dual-targeting agents that interfere with more than one process for parasite survival have shown promise for treating NTDs.[32] For example, quinone−coumarin conjugates and related crassiflorone derivatives possessing activity against parasite glyceraldehyde-3-phosphate dehydrogenase and trypanothione reductase have exhibited micromolar anti-*Trypanosoma* potency at relatively low mammalian host cell cytotoxicity.[33,34] Other dual-targeting agents against trypanothione reductase and iron superoxide dismutase have exhibited micromolar inhibitory effects on *Leishmania donovani* promastigotes.[35] Similarly, cadaverine-anthraquinone conjugates have exhibited effective inhibition against *T. brucei* by interfering with trypanothione reductase, depleting NADPH, and disrupting parasite redox balance by generating reactive oxygen species.[36]

The antimicrobial natural product anisomycin (7, Figure 2) exhibits various activities,[37] but is best known as an inhibitor of translation that blocks ribosome function.[38−41] Considering the subtle structural differences between mammalian and parasite species,[42] and the therapeutic tolerance of anisomycin *in vivo*,[43] the structure−activity relationships of anisomycin have been investigated to improve potency and selectivity. Notably, modification of the aromatic 4-position was shown to preserve antitrypanosomal activity with potential to mitigate host toxicity.[44] In the cocrystal structure of anisomycin bound to the 50S ribosomal subunit of *H. marismortui*,[39] the 4-position of the aromatic ring points toward a hydrophobic crevice in the active site.[39]

Antiprotozoal properties are exhibited by many natural peptides possessing lipophilic acetylene appendages.[47,48] Notably, almiramide B (**10**, Figure 2) exhibits antitrypanosomiasis activity and probable selectivity due to a mechanism of action entailing inactivation of the parasite glycosome, which is an organelle without parallel in mammalian cells.[45,49] Almiramide potency has been attributed in part to the alkyne

https://doi.org/10.1021/acs.jmedchem.5c01291
J. Med. Chem. 2025, 68, 20264−20282

Scheme 1. Synthesis of MeVal[1]- and MePhe[5]-Almiramide−anisomycin Conjugates 18 and 19

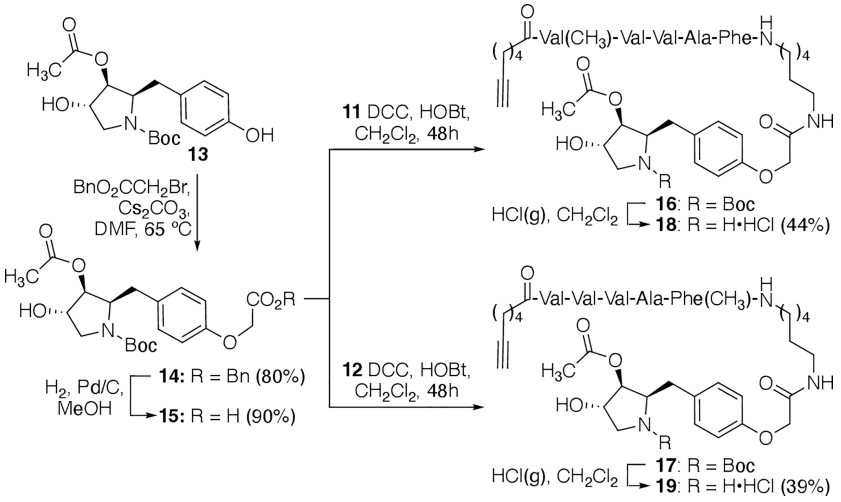

Scheme 2. Synthesis of *p*-Substituted Anisomycin Analogues 20−29

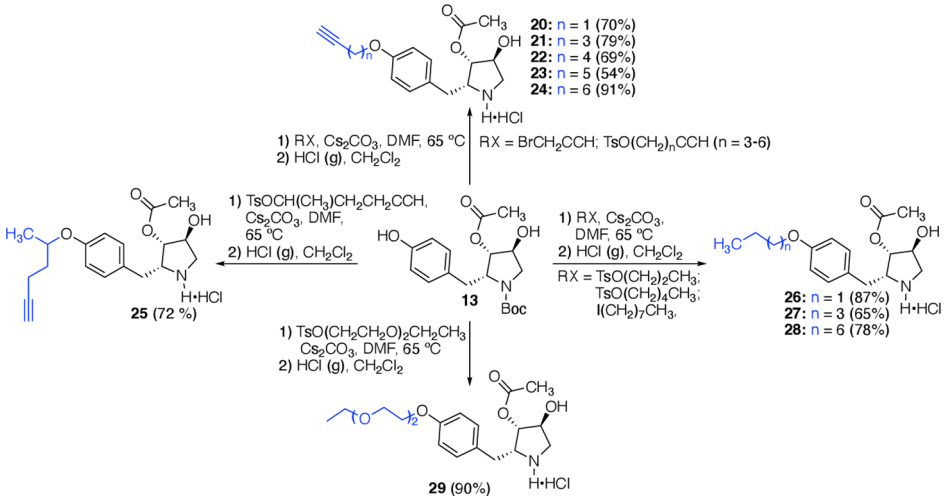

moiety.[45,49] Moreover, structure−activity relationship investigations have provided antileishmanial analogues with efficacy against resistant strains.[46] For example, MeVal[1] and MePhe[5] almiramide 6-aminohexamide derivatives **11** and **12** exhibited notable potency against *Leishmania infantum* wild type and resistant strains.[46]

Exploring the potential to target both the ribosome and the glycosome, two anisomycin−almiramide conjugates were synthesized and examined for activity against *L. infantum* wild type and resistant strains. In a reductionist approach, considering the presence of alkynyl lipid tails in antimicrobial peptides,[47,48] as well as the importance of the acetylene for the antiparasitic activity of almiramide B (**10**),[45,49] different alkynes were grafted onto the *p*-position of the aromatic ring of anisomycin (**7**). Saturated analogues and a polyethylene glycol counterpart were prepared for comparison to study the importance of hydrophobicity and the triple bond for activity. A series of acetylene analogs of anisomycin were identified possessing nanomolar antiparasitic activity against *Leishmania, T. brucei*, and *T. cruzi* species. Certain analogs exhibited improved activity compared to anisomycin against drug-resistant parasite strains. A potent *O*-propargyl analog was shown to exhibit increased potency against amastigote forms of *Leishmania* and to retain a similar ribosomal binding orientation as anisomycin in structural biology studies employing single-particle cryogenic electron microscopy (cryo-EM) analysis (SPA). In concert, genomic analysis validated that the acetylene appendage broadened the mode of action and enabled the targeting of glycosomal proteins. Expanded activity has been achieved by the structure−activity study on anisomycin, indicating a way toward novel therapy for treating trypanosomatid NTDs.

RESULTS

Synthesis of Anisomycin Analogs. Two strategies were pursued to develop dual-targeting agents featuring modification of the aromatic 4-position of anisomycin either by conjugation of the entire almiramide structure via a linker or by attachment of just the alkynyl lipid tail of the peptide. In the first approach, almiramide−anisomycin conjugates **18** and **19** were made using 1,6-hexanediamine as a linker to attach the peptide *C*-terminal carboxylate to a carboxymethyl ether of the phenol of pyrrolidine antibiotic **7**. In studies of the mechanism of almiramide action, related α,ω-diamine linkers were used to conjugate the peptide *C*-terminal carboxylate and biotin in photoaffinity probes that demonstrated binding affinity to the glycosomal membrane proteins GIM5A and PEX11 of *T. brucei*.[45] Considering that MeVal[1] and MePhe[5] almiramide 6-

https://doi.org/10.1021/acs.jmedchem.5c01291
J. Med. Chem. 2025, 68, 20264−20282

Table 1. Structure, Bioactivity (EC_{50}), and Cytotoxicity (CC_{50}) of Anisomycin and *O*-Substituted Analogues on Different Strains of *Leishmania* Promastigotes at 25 °C and Tracking Parasite Replication after 72 h

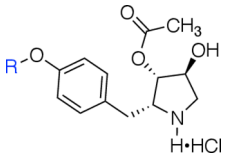

		EC_{50} (μM) (95% CI)						
No.	R	*Li* WT[a]	*Lm*F[b]	*Li*SB-res[c]	*Li*MF-res[d]	*Li*AmB-res[e]	CC_{50} (μM) (BMDM)	SI
1	Miltefosine	0.030 (0.024−0.037)	0.017 (0.011−0.026)	0.081 (0.032−0.169)	>200	0.0667 (0.0419−0.112)	19.3 ± 4.86	643.3
2	Antimony	0.076 (0.683−0.854)	0.066 (0.0456−0.0904)	>2000	0.510 (0.397−0.664)	0.902 (0.756−1.275)	>50	>657.9
7	$-CH_3$	0.238 (0.207−0.276)	0.109 (0.086−0.200)	0.307 (0.264−0.462)	0.467 (0.316−0.507)	0.267 (0.188−0.377)	0.38 ± 0.19	1.6
20	$-CH_2C{\equiv}CH$	0.200 (0.144−0.259)	0.108 (0.084−0.135)	0.130 (0.076−0.250)	0.159 (0.080−0.229)	0.128 (0.980−0.215)	0.55 ± 0.16	2.8
21	$-(CH_2)_3C{\equiv}CH$	0.505 (0.433−0.588)	0.732 (0.575−0.949)	1.301 (0.879−2.185)	0.287 (0.231−0.354)	0.746 (0.555−1.274)	0.36 ± 0.07	0.7
22	$-(CH_2)_4C{\equiv}CH$	0.408 (0.284−0.554)	0.414 (0.2745−0.711)	16.80 (11.43−24.96)	10.74 (7.953−14.55)	0.641 (0.478−0.962)	0.51 ± 0.50	1.3
23	$-(CH_2)_5C{\equiv}CH$	0.784 (0.650−0.956)	0.756 (0.574−1.651)	1.201 (0.885−1.776)	0.553 (0.481−0.635)	0.832 (0.701−1.057)	1.32 ± 0.19	1.8
24	$-(CH_2)_6C{\equiv}CH$	1.875 (0.858−7.597)	2.136 (0.895−6.888)	0.578 (0.498−0.673)	0.497 (0.438−0.565)	0.767 (0.639−0.951)	1.20 ± 0.20	0.6
25	$-CCH_3H(CH_2)_2C{\equiv}CH$	1.883 (0.892−7.493)	2.253 (0.894−11.58)	1.154 (0.887−1.621)	0.673 (0.592−0.769)	1.015 (0.909−2.051)	0.61 ± 0.05	0.3
26	$-CH_2CH_2CH_3$	1.558 (0.626−5.441)	2.538 (0.891−11.27)	0.482 (0.424−0.547)	0.336 (0.300−0.375)	0.568 (0.459−0.695)	0.29 ± 0.06	0.2
27	$-(CH_2)_3CH_2CH_3$	2.933 (0.976−11.05)	3.257 (1.398−7.614)	1.006 (0.807−1.381)	0.682 (0.619−0.754)	1.023 (0.875- 2.051)	1.00 ± 0.10	0.3
28	$-(CH_2)_6CH_2CH_3$	7.163 (5.678−10.32)	3.638 (1.267−6.879)	11.33 (5.525−21−26)	2.879 (1.484−3.765)	2.323 (1.683−3.573)	22.85 ± 5.98	3.2
29	$-(CH_2CH_2O)_2CH_2CH_3$	13.780 (7.640−35.21)	8.943 (5.655−16.30)	17.67 (12.26−24.96)	1.475 (1.208−1.871)	5.851 (2.673−12.380)	0.94 ± 0.05	0.1

[a]*Leishmania infantum* (MHOM/MA/67/ITMAP-263) wild-type strain. [b]*Leishmania major* Friedlin; *Leishmania infantum* (MHOM/MA/67/ITMAP-263). [c]Resistant to 2 mM trivalent (and pentavalent) antimonials. [d]200 μM miltefosine. [e]1 μM amphotericin B. Selectivity index (SI) = CC_{50}/EC_{50} *Li*WT.

aminohexamides **11** and **12**, as well as *p*-carboxymethyl anisomycin **9**, all exhibited antileishmanial activity,[44,46] conjugation of the two components was examined in an expedient design to test the first strategy.

4-Carboxymethyl *N*-(Boc)anisomycin **15** was prepared in 90% overall yield from *N*-Boc-desmethylanisomycin (**13**) and benzyl bromoacetate in two steps featuring Williamson ether synthesis using cesium carbonate and hydrogenolysis of *O*-benzyl ester **14** using catalytic Pd/C under 1 atm of H_2 (Scheme 1). Amiramide−anisomycin conjugates **18** and **19** were, respectively, synthesized by routes entailing the coupling of 4-carboxymethyl *N*-(Boc)anisomycin **15** to almiramide hexyl amines **10** and **11** using *N*,*N*′-dicyclohexylcarbodiimide (DCC) and 1-hydroxybenzotriazole (HOBt) in dichloromethane, purification of the resulting conjugates **16** and **17** by C18 reverse-phase HPLC, and removal of the Boc protection using HCl gas bubbles in CH_2Cl_2 [Supporting Informmation (Table S4)].

In the second strategy, the terminal acetylene motif was considered sufficient to disrupt the glycosomal function. *O*-Alkynyl anisomycin analogues **20**−**24** were prepared by way of alkylation of phenol **13** using Cs_2CO_3 in DMF at 65 °C with propargyl bromide and primary *p*-toluenesulfonates of five to eight carbon chain lengths (Scheme 2). Based on the submicromolar antileishmanial activity of *O*-*iso*-propyl anisomycin (**8**, Figure 2),[44] *O*-1-methylpentyne counterpart **25** was prepared using branched hex-5-yn-2-yl-toluenesulfonate under similar conditions. For comparisons, *O*-*n*-alkyl anisomycins **26**−**28** were prepared using the same protocol with *n*-propyl and *n*-pentyl toluenesulfonates and octyl iodide to examine the importance of lipophilic tails of 3-, 5-, and 8-carbons, and *O*-2-(2-ethoxyethoxy)ethyl anisomycin **29** was prepared as a more polar 8-atom chain by employing the corresponding toluenesulfonate. After phenol alkylation, the Boc group was removed using a slow stream of HCl gas bubbles in CH_2Cl_2, because vigorous bubbling led to the formation of demethylanisomycin hydrochloride and desacetyl product, which required removal by HPLC, compromising the product yield. After deprotection, ethers **20**−**29** were isolated as hydrochloride salts (Table S4).

Anti-Parasitic Activity. Antileishmanial activity (EC_{50} values) was assessed by incubation of increasing concentrations of anisomysin−almiramide conjugates and *p*-substituted anisomycin analogues with *Leishmania* spp. promastigotes at 25 °C and tracking parasite replication after 72 h (Table 1).[44] Cytotoxicity was evaluated using bone-marrow-derived macrophages (BMDM).

Against *Leishmania* (*L.*) *infantum* wild type and strains resistant to antimony (SbIII), amphotericin B (AmB), and miltefosine (MF) (Sb2000.1, AmB1000.1, and MF200.5), MeVal[1] and MePhe[5] almiramide derivatives **11** and **12** were previously shown to exhibit EC_{50} values ranging between 5 and 39 μM.[46] Anisomycin (**7**) was first shown to inhibit translation

https://doi.org/10.1021/acs.jmedchem.5c01291
J. Med. Chem. 2025, 68, 20264−20282

Table 2. Activity (EC_{50}) and Cytotoxicity (CC_{50}) of *p*-Substituted Anisomycin Analogues 20−29 against *T. brucei* Promastigotes and *T. cruzi* Epimastigotes

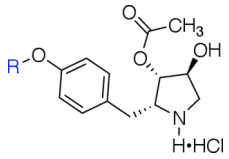

No.	R	*T. brucei*[a] EC_{50} (μM)	*T. cruzi*[b] EC_{50} (μM)	CC_{50} (μM) (BMDM)	SI[a]	SI[b]
4	pentamidine	1.58 ± 0.033	3.25 ± 1.205	13.61 ± 1.33	8.6	4.2
7	$-CH_3$	0.090 ± 0.007	0.321 ± 0.09	0.38 ± 0.19	4.2	1.2
20	$--CH_2C{\equiv}CH$	0.613 ± 0.053	1.507 ± 0.25	0.55 ± 0.16	0.9	0.4
21	$-(CH_2)_3C{\equiv}CH$	0.154 ± 0.021	0.207 ± 0.094	0.36 ± 0.07	2.3	1.7
22	$-(CH_2)_4C{\equiv}CH$	0.21 ± 0.01	0.39 ± 0.026	0.51 ± 0.5	2.4	1.3
23	$-(CH_2)_5C{\equiv}CH$	0.38 ± 0.001	0.92 ± 0.07	1.32 ± 0.19	3.5	1.4
24	$-(CH_2)_6C{\equiv}CH$	0.37 ± 0.05	0.97 ± 0.07	1.2 ± 0.2	3.2	1.2
25	$-CCH_3H(CH_2)_2C{\equiv}CH$	0.38 ± 0.07	1.11 ± 0.2	0.61 ± 0.05	1.6	0.5
26	$-CH_2CH_2CH_3$	0.18 ± 0.02	0.46 ± 0.04	0.29 ± 0.06	1.6	0.6
27	$-(CH_2)_3CH_2CH_3$	0.39 ± 0.06	0.97 ± 0.2	1.0 ± 0.1	2.5	1.0
28	$-(CH_2)_6CH_2CH_3$	2.78 ± 0.244	4.93 ± 0.682	22.85 ± 5.98	8.2	4.6
29	$-(CH_2CH_2O)_2CH_2CH_3$	1.92 ± 0.53	5.8 ± 3.00	0.94 ± 0.05	0.5	0.2

[a]*Trypanosoma brucei*. [b]*Trypnosoma cruzi*; SI = CC_{50}/EC_{50}.

in *Leishmania tarentolae* (EC_{50} = 0.55 ± 0.16 μM).[44] In studies of antipromastigote activity, anisomycin (**7**) exhibited antileishmanial activity with EC_{50} values in the submicromolar range against *L. infantum* and resistant strains.[44] In contrast, no activity was exhibited by conjugates **18** and **19** composed, respectively, of anisomycin (**7**) and almiramides **11** and **12**.

Conversely, *p*-substituted anisomycin analogs exhibited significant antileishmanial activity contingent on the *p*-substituent (Table 1). *O*-Propargyl ether **20** exhibited, respectively, comparable nanomolar activity as anisomycin against *L. infantum* wild type (*Li*WT) and *Leishmania major* (*LmF*). Although submicromolar potency was typically retained, the activity of the linear acetylene analogs decreased progressively with the increasing chain length. Moreover, the branched analogue **25** exhibited 8-fold less activity against *Li*WT relative to anisomycin. The importance of the terminal alkyne was reflected in the lower potency upon replacing acetylene tails with saturated counterparts **26**−**28**. For example, *O*-*n*-propyl anisomycin **26** was, respectively, 7- and 23-fold less potent against *Li*WT and *LmF* compared to *O*-propargyl anisomycin **20**. Similarly, *O*-pentyl and *O*-octyl ethers **27** and **28** were, respectively, 12- and 30-fold less potent against *Li*WT compared to similar carbon chain-length acetylene counterparts **21** and **24**. The crucial role of hydrophobicity for ribosomal targeting was respectively illustrated by the 7- and 2-fold lower potency of *O*-di(ethylene glycol)ethyl ether **29** compared to *O*-oct-7-ynyl and *O*-octyl ethers **24** and **28**.[39,44]

The acetylene modification typically improved potency against drug-resistant strains *Li*MF200.5, *Li*SB2000.1, and *Li*AmB1000.1, which are resistant to MF, Sb, and AmB, respectively. For example, *O*-propargyl ether **20** exhibited between 2.4, 3.0, and 2.1-fold greater potency than anisomycin (**7**) against the Sb-, MF-, and AmB-resistant strains. Moreover, the presence of the acetylene in analogs **20**, **21**, and **24** gave between 0.8- to 19.6-fold greater potency than the respective *O*-*n*-propyl, *O*-pentyl, and *O*-octyl ethers **26**−**28** against the drug-resistant strains.

The antitrypanosomal activity of anisomycin analogues **20**−**29** was further evaluated against *T. brucei* promastigotes and *T. cruzi* epimastigotes using pentamidine (**4**) as the positive control (Table 2). The epimastigote form of *T. cruzi* is considered an obligate mammalian intracellular stage,[50,51] which is commonly used to screen for potential antichagasic agents with a criterion of identifying high potency around 10 μM, and low toxicity with an SI that is 50 times higher than that of the reference drug.[52] Conjugates **18** and **19** were not tested against *T. brucei* and *T. cruzi*, due to the absence of activity of the parent almiramide peptides **11** and **12**.[46]

Anisomycin (**7**) exhibited, respectively, 90 nM and 321 nM EC_{50} values against *T. brucei* and *T. cruzi*. Among the *O*-substituted anisomycin analogs, *O*-pent-4-yne ether **21** retained comparably robust activity, exhibiting respectively 1.7-fold lower and 1.5-fold higher potencies as anisomycin against *T. brucei* and *T. cruzi*. Moreover, *O*-hex-5-yne ether **22** maintained similar activity as anisomycin against *T. cruzi*. Despite the favorable activity of the 5- and 6-carbon alkynyl ethers **21** and **22** against *T. cruzi*, and comparable macrophage toxicity as anisomycin, the low selectivity indexes of 1.7 and 1.3 did not merit further study in the amastigote form. Per observations of activity against *Leishmania*, antitrypanosomal potency decreased with increasing chain length; however, *O*-propargyl ether **20**, which exhibited the best activities against *Li*WT and *Lm*F had, respectively, 4- and 7-fold lower activity than *O*-pent-4-yne ether **21** against *T. brucei* and *T. cruzi*. Furthermore, propyl ether **26** was 1.4- and 2-fold less active than anisomycin against *T. brucei* and *T. cruzi*. In *O*-*n*-alkyl ethers of longer chain lengths, the importance of acetylene for activity was demonstrated. Compared to acetylene counterparts **21** and **24**, *O*-*n*-pentyl and *O*-*n*-octyl analogues **27** and **28** displayed, respectively, 2.5- and 7.5-fold lower activity against *T. brucei* and were both 5-fold less active against *T. cruzi*. Moreover, *O*-di(ethylene glycol)ethyl ether **29** was 5- and 6-fold less potent than its *O*-oct-7-ynyl counterpart **24**.

Effect of *O*-Propargyl Ether 20 on *Leishmania* Amastigotes. The high activity of *O*-propargyl ether **20** against *Leishmania* promastigotes evoked a study of the efficacy against the amastigote intracellular form of the parasite (Figure 3). Compared to the activity against that promastigote form, *O*-

https://doi.org/10.1021/acs.jmedchem.5c01291
J. Med. Chem. 2025, 68, 20264−20282

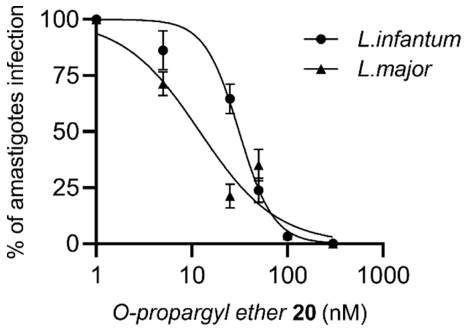

Figure 3. Effect of *O*-propargyl ether **20** on BMDM macrophages infected with *L. infantum* wild type (WT) and *L. major*.

propargyl ether **20** showed 6- and 8-fold increases in potency against the amastigote forms of *L. infantum* and *L. major* with respective EC_{50} values of 31.22 nM (95% CI 25.44−36.28) and 12.08 nM (95% CI 7.64−18.57). *O*-Propargyl ether **20** maintained its potency against both parasite stages, indicating therapeutic potential.

Cryo-EM Analysis of *Leishmania* Ribosomes Bound to *O*-Propargyl Ether 20. Previously, the cocrystal structure of anisomycin bound to the 50S ribosomal subunit of *H. marismortui* demonstrated that the pyrrolidine nitrogen forms hydrogen bonds with the N3 of cytosine 2487 (*H. marismortui* numbering). The latter base also stacks against the aromatic ring of the *p*-methoxyphenyl group of anisomycin.[39] Furthermore, the anisomycin hydroxyl group interacted with the nonbridging oxygen of Uracil 2539 (*H. marismortui* numbering) nucleotide phosphate.[39]

Structural analysis using SPA was performed to elucidate the mechanism by which *O*-propargyl ether **20** inhibits translation in *Leishmania*. A 2.5 Å resolution cryo-EM structure was obtained for the complex between intact cytosolic *L. major* 80S ribosomes, mRNA, tRNA, and *O*-propargyl ether **20**. A well-defined density was observed for *O*-propargyl ether **20** near the peptidyl transferase center (PTC, Figure 4A, Video S1). The

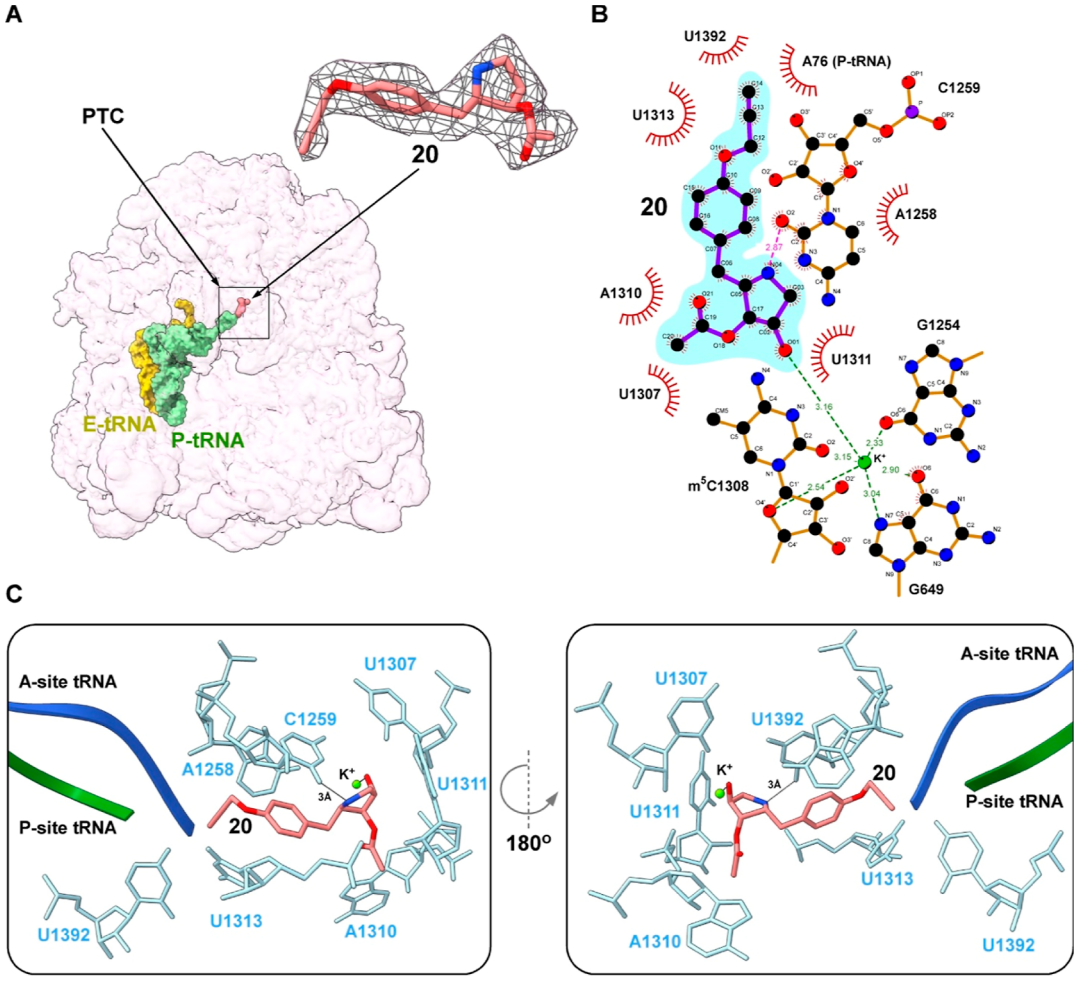

Figure 4. Part of the cryo-EM structure of *L. major* 80S ribosome to which *O*-propargyl ether **20** is bound. (**A**) Location of ether **20** in *L. major* 80S PTC. The E- and P-site tRNA are shown as space-filling colored in yellow and green, respectively. An inset showing the EM density of ether **20** is presented as a meshed surface. (**B**) Ether **20** interaction with the rRNA nucleotides, created using LigPlot+. Hydrogen bonds, ion coordination, and hydrophobic interactions are, respectively, shown with dotted purple lines, dotted green lines, and red crescents. The rRNA nucleotides making hydrogen bonds with ether **20** and coordinating the K^+ ion are shown using their complete chemical structure diagrams. Nucleotides exhibiting hydrophobic interactions are depicted as labeled red crescents. (**C**) Graphical images showing two perspectives of the three-dimensional binding pocket into which ether **20** (pink) interacts with proximal rRNA nucleotides (light blue) within P-site tRNA (green ribbon), neighboring A-site tRNA (blue ribbon). *L. major* A-site tRNA (blue ribbon) was superimposed from PDB: 8RXH. The hydrogen bond between ether **20** and rRNA nucleotide, and coordination of K^+ ion (green ball) are shown as dotted lines.

https://doi.org/10.1021/acs.jmedchem.5c01291
J. Med. Chem. 2025, 68, 20264−20282

high resolution of the cryo-EM map enabled us to model the LM80S-**20** complex structure, featuring the entire *L. major* rRNA, proteins (rRNA and rProteins), and *O*-propargyl ether **20**.

Comparison of the LM80S-**20** structure with our previously published vacant *L. major* 80S ribosome (LM80S, PDB: 8OVJ) and the postdecoding pretranslocation state (PDB: 8RXH) indicated similar overall architecture.[53] Superimposition of the LM80S-**20** structure with the human 80S ribosomes bound to anisomycin (**7**, PDB: 8GLP) revealed a highly conserved binding pocket (Figure S1A). Minor structural differences were observed for U1392 [Ψ4531 in Human, Figure S1B (left panel)] and U1260 [U4399 in Human, Figure S1B (right panel)].

The high-resolution cryo-EM map enabled the identification of potential interactions between *O*-propargyl ether **20** and surrounding rRNA nucleotides. A stacking interaction was observed between the aromatic ring of the *p*-alkoxyphenyl group of ether **20** and cytosine-1259 (C2487 in *H. marismortui* or C2452 in *E. coli*), as previously observed for the *p*-methoxyphenyl moiety of anisomycin (**7**) bound in the crystal structure to *H. marismortui* 50S ribosome (Figure 4B,C).[39] The rRNA nucleotides in close contact with *O*-propargyl ether **20** are presented in Figure 4B. The high resolution of the EM map enabled detection of a potential coordination between the hydroxyl group of ether **20** (O1) and a neighboring potassium ion (Figure 4B,C). A similar coordination of a potassium ion was also observed in the human 80S complex with anisomycin (**7**) (PDB: 8GLP). Ion coordination by the hydroxyl group may stabilize ribosomal affinity.[54,55]

Thermal-Proteome Profiling (TPP) of Proteins Targeted by Anisomycin (7) and *O*-propargyl Ether 20 Indicates a Mechanism of Action Broadening from Ribosomal to Include Glycosomal Pathways. TPP is an established, unbiased approach in which ligand-induced shifts in protein melting behavior are quantified by mass spectrometry to reveal direct and stoichiometric drug−protein interactions.[56] Using TPP on *L. infantum* wild-type (*Li*WT) promastigotes, 2768 and 2503 proteins were respectively quantified after treatment with anisomycin (**7**) and with *O*-propargyl ether **20**. Thermal-stability shifts $|\Delta T_m| > 4$ °C were, respectively, shown in 253 and 423 proteins from the latter sets (Figure 5A; Tables S1 and S2). Both anisomycin (**7**) and ether **20** gave similar signatures on ribosomal proteins (Figure 5B). Large positive ΔT_m values were recorded for ubiquitin-60S L40 and more than 20 small- and large-subunit proteins, including S16, S6, L3, L7a, and L18, indicating direct engagement of the translation apparatus. This pattern was consistent with the canonical mechanism of anisomycin, which binds the peptidyl-transferase center of the 60S subunit and blocks peptide-bond formation. The indistinguishable ribosomal footprint of ether **20** indicated an analogous primary mode of binding.

O-Propargyl ether **20** was found to be directly bound or to allosterically modulate certain enzymes involved in glycolysis and glycosomal metabolism, such as glyceraldehyde-3-phosphate dehydrogenase (A4IDK9), and glucose-6-phosphate isomerase (E9AGE1), as well as to stabilize purine metabolism enzymes, such as hypoxanthine phosphoribosyltransferase (E9AGU6). The thermal shifts suggested that, in addition to translation, ether **20** influenced metabolic processes linked to energy production and redox balance by engaging glycosomal proteins implicated in the first steps of glycolysis and key branches of central carbon metabolism within *Leishmania*.

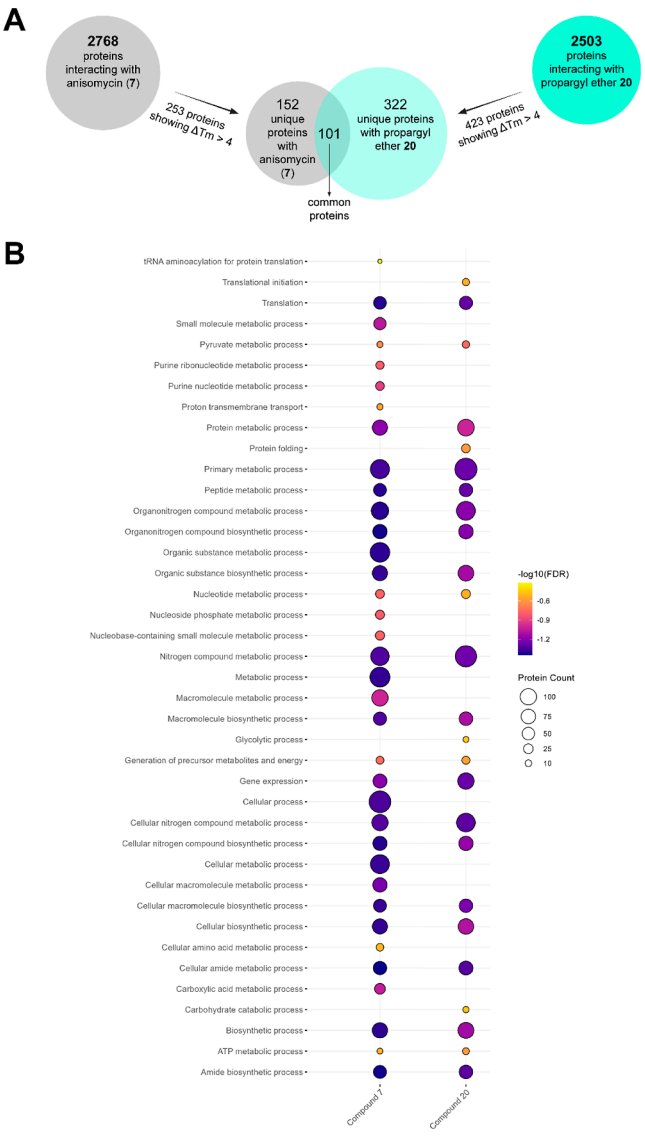

Figure 5. Proteome-wide targets of anisomycin (**7**) and *O*-propargyl ether **20** in *Leishmania infantum* promastigotes were identified by TPP. Proteins exhibiting a thermal-stability shift of ≥4 °C ($|\Delta T_m|$) after drug exposure were considered engaged targets. (**A**) Venn diagram summarizing the number of proteins in which anisomycin (gray) and ether **20** (cyan) significantly altered melting behavior; the overlap denotes proteins affected by both compounds. (**B**) Gene-ontology (GO) enrichment of the drug-responsive proteins is depicted as a bubble plot. The bubble area is proportional to the number of proteins annotated to a given GO biological-process term. Color encodes statistical significance [false-discovery rate in log scale, $-\log_{10}(\text{FDR})$]: purple and yellow indicate the most and least significant enrichments, respectively.

The premise that ether **20** exhibited a broader mode of action was reinforced by GO over-representation analysis. Proteins destabilized or stabilized by both compounds were enriched for processes such as “translation”, “ribosome biogenesis”, and “tRNA amino-acylation”. The cohort specifically influenced by ether **20** was enriched in proteins for “glycolytic process”, “pyruvate metabolic process”, and “carbohydrate catabolic process”. Anisomycin and ether **20** share the ribosome as a principal molecular target (Figure 6A), but the propargyl modification introduced a second pharmacological node inside

https://doi.org/10.1021/acs.jmedchem.5c01291
J. Med. Chem. 2025, 68, 20264−20282

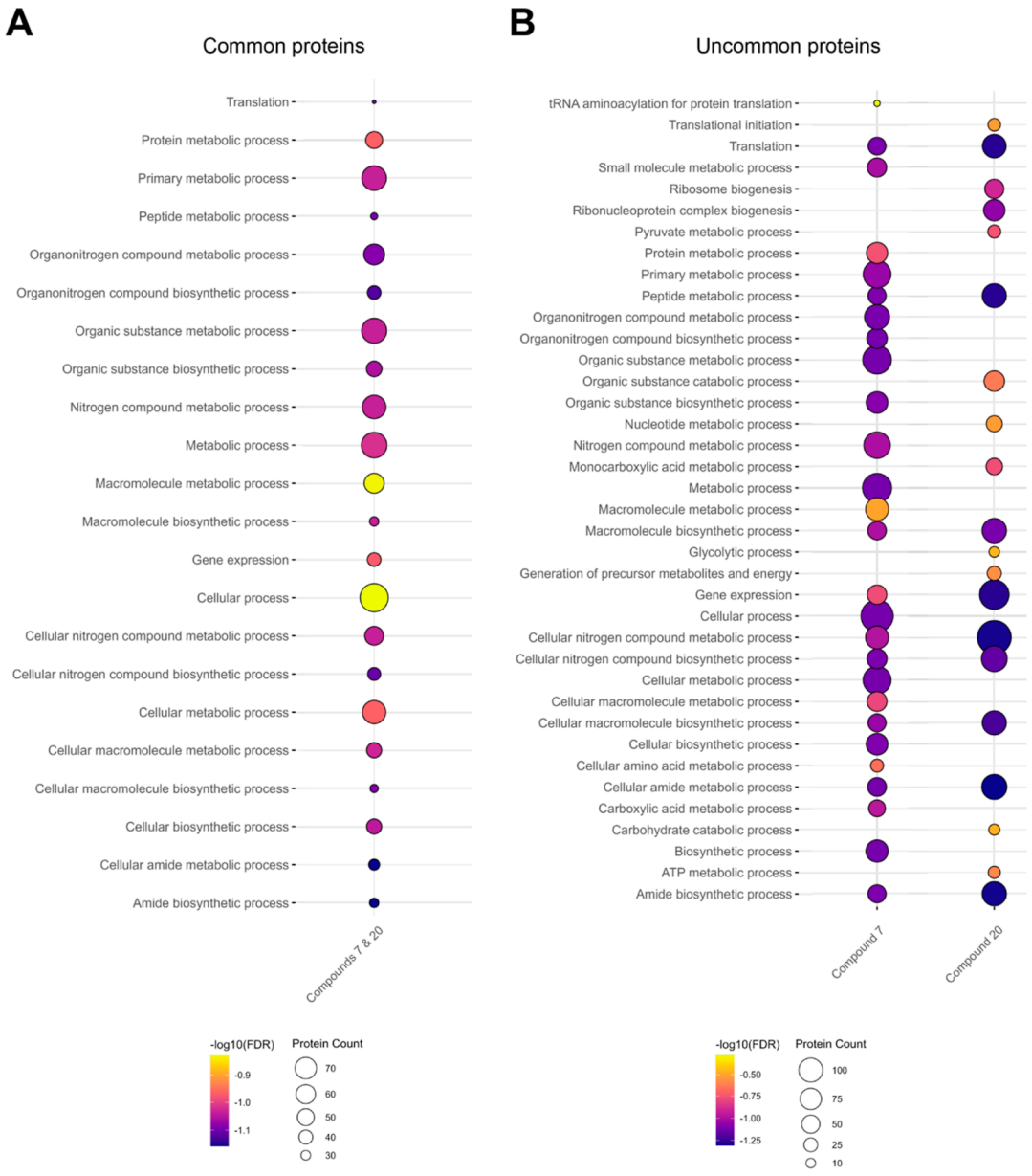

Figure 6. GO landscape of drug-responsive proteins in *Leishmania infantum* identified by TPP. Promastigotes were exposed to anisomycin (**7**) or *O*-propargyl ether **20**, and proteins showing a thermal stability shift of ≥4 °C were identified as candidate drug interactors. Bubble plots depict GO enrichment based on these candidates. (**A**) Terms enriched in the protein subset shared by both compounds. (**B**) Terms enriched in proteins uniquely affected by either anisomycin (**7**) or ether **20**. For each GO term, the bubble area scale corresponds with the number of annotated proteins; bubble color denotes enrichment significance [FDR in log scale, $-\log_{10}$(FDR)]: purple and yellow indicate the most and least significant enrichments, respectively.

the glycosome (Figure 6B), which may disrupt metabolic fluxes essential for parasite viability.

DISCUSSION AND CONCLUSIONS

In the treatment of trypanosomatid infection, resistance has diminished the efficacy of contemporary therapies, which typically target a single point of intervention.[57] Although combination therapy has shown some promise,[57] single chemical entities targeting multiple points of intervention may evade resistance and offer advantages for minimizing drug−drug interactions and improving compliance.[27,31] In this context, the ribosome and glycosome are both vital for the parasite lifecycle. Previously, replacement of the methyl ether of the ribosomal inhibitor anisomycin (**7**) in *O*-isopropyl counterpart **8** improved selectivity for inhibiting translation in *Leishmania* vs rabbit reticulocytes.[44] Disruption of the vital energy machinery proteins of the glycosome was implicated in the mechanism of action of almiramide peptides by studies employing various linkers attached at the *C*-terminal in different probes, some retaining activity.[45] Structure−activity relationship studies have previously shown the relevance of the acetylene in the lipid tail for the activity of almiramide B (**10**),[49] as well as retained potency in peptides **11** and **12** in which certain *N*-methyl groups were removed from the amide backbone and a 6-amino hexanamide was added to the *C*-terminal.[46] Anisomycin-almiramide conjugates **18** and **19** exhibited potency poorer than that of the parent components. Previously, conjugates from anisomycin and sparsomycin exhibited lower antimicrobial

https://doi.org/10.1021/acs.jmedchem.5c01291
J. Med. Chem. 2025, 68, 20264−20282

activity but enhanced inhibitory activity against translation in rabbit reticulocytes relative to the parent components.[58] These examples reveal the challenges in conjugate design, which is contingent on various variables including linker composition and the points of attachment of the parent components, and argue for structural simplification.[59]

The acetylene moiety is present in the lipid tails of various antimicrobial peptides such as almiramide B. In a reductionist approach, alkyne analogs were prepared and, in some instances, exhibited similar antitrypanosomatid activity as anisomycin (7). Versus *Leishmania*, *O*-propargyl ether **20** exhibited comparable activity as anisomycin (7) against *L. infantum* and *L. major*, as well as superior activity in resistant *L. infantum* strains. Moreover, *O*-pentynyl ether **21** maintained activity in *L. major* and *Li*MF-resistant strains but was less active in *Li*SB-resistant strains. Although potency and selectivity declined in the longer chain alkynes **22**−**25**, the triple bond analogs typically manifested about 4−8-fold better activity than saturated counterparts **26**−**28** and were superior to relatively hydrophilic *O*-di(ethylene glycol)ethyl ether **29**, which exhibited the poorest activity.

O-pentynyl ether **21** exhibited equivalent activity as anisomycin versus *T. brucei* and *T. cruzi*. Moreover, *O*-hexynyl ether **22**, *O*-heptynyl ether **23**, and branched alkyne **25** showed moderate activity in *T. brucei* and slightly lower activity in *T. cruzi*. Although the low activity of *O*-propargyl and propyl ethers **20** and **26** in the trypanosomal assay is puzzling, the alkyne and lipophilicity remain essential for activity.

Acetylene groups have been widely utilized in medicinal chemistry, including prominent examples in clinically used anticancer and contraceptive agents.[60] The alkyne can serve as a π cloud, and the polarized terminal CH may act as a weak hydrogen-bond donor. On the other hand, acetylene is potentially reactive toward oxidation by cytochrome P450 enzymes and attack from glutathione.[60] Structural analyses of *O*-propargyl ether **20** and anisomycin (7) in ribosomal complexes using cryo-EM indicated that the acetylene did not influence the binding motif to the **conserved** peptidyl transferase **pocket** (Figure 4). The enhanced potency of the acetylene analogs of anisomycin is likely due to a broader mode of action, as indicated by thermal proteomic profiling experiments.

O-Propargyl ether **20** demonstrated 2- to 3-fold greater potency against antimony-, miltefosine-, and amphotericin-resistant *Li*-strains. To evade drug action, resistant *Leishmania* strains utilize various mechanisms that typically reduce the active drug concentration within the parasite.[61] For example, antimony-resistant *Leishmania* strains overexpress tryparedoxin peroxidase to mitigate stress due to reactive oxygen and nitrogen species induced by antimonial drugs.[62] Moreover, the expression patterns of enzymes involved in glycolysis and energy metabolism in the glycosome, such as glucose-6-phosphate isomerase and glyceraldehyde-3-phosphate dehydrogenase, are often altered in antimony-resistant parasites.[61] Apoptotic pathways induced by miltefosine and amphotericin have also been inactivated by expression of multiple heat shock protein 70 (HSP70) isoforms in resistant *Leishmania* strains.[63] Overexpression of protein HSP83 correlated with reduced susceptibility to Sb(V) in resistant strains by maintaining mitochondrial potential.[64]

The thermal proteomic profiling correlates the superior activity of propargyl ether **20** against resistant strains compared to anisomycin (7) with the engagement of a broader group of protein targets, specifically those implicated in glycosomal activity. For example, glyceraldehyde-3-phosphate dehydrogenase (A4I5X6), as well as heat shock proteins 70 and 83, were selectively targeted by propargyl ether **20**. Furthermore, ether **20** interacted with the DEAD-box RNA helicase, a regulator of parasite survival that suppresses apoptosis-like programmed cell death (Table S2).[65] GO and pathway enrichment analyses indicate that glycolytic and catabolic processes are influenced explicitly by ether **20**.

The promastigotes of *Leishmania* are in the insect stage, which is the form that develops and multiplies within the sandfly vector. Genetic variants of the promastigotes are easier to cultivate and screen to study structure−activity relationships; however, the amastigotes are the intracellular, nonmotile form found in human macrophages, and the clinically relevant stage for validating mammalian antiparasitic activity.[66] The effect of *O*-propargyl ether **20** was further evaluated against intracellular *L. infantum* and *L. major* amastigotes.[63] Dose response studies revealed that *O*-propargyl ether **20** exerted 6- and 8-fold increased activity against the amastigotes. Such potency indicated potential to penetrate the host cell and overcome protective mechanisms such as phagolysosomal activity, lower pH, and oxidative degradation.[66,67]

The addition of acetylenic ethers to the ribosomal inhibitor anisomycin (7) has provided analogs possessing improved activity against trypanosomatid parasites, especially resistant *Leishmania* strains. Examining the ribosomal complex with potent *O*-propargyl ether **20** by using cryo-EM techniques indicated that the aromatic ring modification had no consequence on the binding motif of the substituted pyrrolidine structure. On the other hand, TPP revealed that the acetylene appendage expanded the mode of action of the parent natural product. Novel interactions were identified, accounting for the improved activity against resistant parasites known to modify the expression of glycosomal proteins in response to contemporary therapy. Further studies of this approach, including validation of lead potential *in vivo*, are being performed and will be reported in due time. Toward addressing the need for therapy to treat NTDs caused by trypanosomatid parasites, the present strategy to create multiple targeting ligands based on anisomycin has identified promising agents for targeting *Leishmania*, *T. brucei*, and *T. cruzi*.

EXPERIMENTAL SECTION

Materials and Methods. *Chemistry. Solvents.* Passage through filtration systems (GlassContour Irvine, CA) was employed to dry reaction solvents: dichloromethane (DCM), acetonitrile, and dimethylformamide (DMF). Hexanes (Fischer, ACS grade) were fractionally distilled. Ethyl acetate, diethyl ether (Fisher, BHT stabilized, ACS grade), and methanol (Fisher, ACS grade) were used as received.

Reagents. *p*-Toluene sulfonic acid (PTSA) was recrystallized from EtOH and water. Boron tribromide (Sigma-Aldrich), di-*tert*-butyldicarbonate (Boc_2O, Oakwood Chemicals), triethyl amine (Oakwood Chemicals), 4-dimethylamino pyridine (DMAP, Aldrich), *N*,*N*′-dicyclohexylcarbodiimide (DCC, Aldrich), hydroxybenzotriazole (HOBt, Aldrich), 4-pentyn-1-ol (Aldrich), 5-hexyn-1-ol (Oakwood Chemical), 7-octyn-1-ol (Aldrich), propyl alcohol, and pentyl alcohol were used as received. Hept-6-yn-1-ol,[68] hex-5-yn-2-ol,[69] benzyl bromoacetate[70] were prepared according to the literature protocols. Propargyl bromide and octyl iodide were passed through a pad of silica gel (Silicycle SiliaFlashP60, 40−63 μm particle size, 230−400 mesh) immediately prior to use. Cesium carbonate (Cs_2CO_3) was flame-dried in a round-bottom flask under vacuum using a Bunsen burner prior to use.

Chromatography. Analytical thin-layer chromatography (TLC) was performed on Merck silica gel 60G F254 plates, which were

https://doi.org/10.1021/acs.jmedchem.5c01291
J. Med. Chem. 2025, 68, 20264−20282

visualized by exposure to ultraviolet (UV) light (254 nm), ninhydrin ethanol solution, aqueous $KMnO_4$, and ceric ammonium molybdate. Retention factor (R_f) values were measured after elution on a 6 × 4 cm TLC plate in a developing chamber containing the described solvent system. Flash column chromatography was performed on silica gel (Silicycle SiliaFlashP60, 40−63 μm particle size, 230−400 mesh).[71] High-performance liquid column chromatography (HPLC) was performed on a Waters C18 column (SunFire, particle size, 10 μm, 150 mm × 10 mm) with detection at 214 nm using a linear gradient of 0−10% over 10 min, 10−90% over 20 min, followed by 10% (v/v) of MeOH [0.1% formic acid (FA)] in water (0.1% FA) with a flow rate of 4.2 mL min^{-1} (Table S5). Unless otherwise specified, "silica gel" refers to P60 grade.

pH Measurements. pH was determined using MQuant pH-indicator strips (nonbleeding, pH 0.0 to 14.0).

NMR spectroscopy: ^1H and $^{13}C\{^1H\}$ NMR spectra were recorded at 298.2 K on a Bruker AVANCE NEO 400 MHz (400 MHz, ^1H; 100 MHz, $^{13}C\{^1H\}$)spectrometer and are referenced to residual chloroform-*d* (δ 7.26 ppm, ^1H; 77.16 ppm, $^{13}C\{^1H\}$), methanol-d_4 (3.31 ppm, ^1H; 49.00 ppm, $^{13}C\{^1H\}$), and water-d_2 (δ 4.79 ppm, ^1H). Chemical shifts (δ) are reported in parts per million (ppm), and coupling constant values (*J*) are reported in Hertz (Hz). Abbreviations—s, singlet; d, doublet; t, triplet; q, quartet; quint, quintet; sext, sextet; br, broad; m, multiplet.

Mass Spectrometry. Liquid chromatography−mass spectrometry (LC−MS) was performed using an Agilent series symmetry C18 column (3.5 μm 4.6 × 75 mm) maintained between 27 and 30 °C and 118.7 and 141.5 bar using a flow rate of 0.7 mL min^{-1} or 0.8 mL min^{-1}. An ES-API ionization source with both positive and negative ionization polarity and 5.0 V ionization energy were employed as MSD parameters. Data are reported in the form of *m*/*z* (intensity relative to the base peak = 100). The mobile phase consisted of (A) H_2O containing 0.1% FA in (B) either MeOH containing 0.1% FA or MeCN containing 0.1% FA. The gradient elution started with 10% of phase B for 2 min was gradually increased over 10 min to B = 90% and held at 90% for 1 min. The column was then equilibrated with the initial conditions at 10% B for 3 min (14 min per run in total). The purity was determined with MeOH and MeCN at wavelengths of either 214 or 220 nm employing a UV/visible diode array detector. Except for compound **18** (91% in MeCN), the compounds exhibited ≥95% purity in both solvent systems (Table S4).

Biology. Ethical Statement. Experimental protocols were approved by the Facility Animal Care Committee, Research Institute MUHC (protocol number 7791). The Canadian Council on Animal Care guidelines and regulations were followed for all mice used in the experiments, including handling and housing under specific pathogen-free conditions.

Leishmania Cultures. Multiple *Leishmania* lines were used, including the *L. infantum* (MHOM/MA/67/ITMAP-263) and *L. major* (LV39 WT) wild-type strains and three drug-resistant mutants (*Li*Sb2000.1, *Li*AmB1000.1, and *Li*MF200.5), which were generated through stepwise selection with potassium antimonyl tartrate (Sb), amphotericin B (AmB), and miltefosine (MF).[72−75] All *Leishmania* lines were continuously cultured in M199 medium supplemented with 10% fetal bovine serum, 5 μg/mL hemin, adjusted to pH 7.0, at 25 °C. Drug resistance was maintained by supplementing the medium with the corresponding EC_{50} concentrations for each mutant: 2 mM Sb (Sigma-Aldrich no. 383376) for *Li*Sb2000.1, 1 μM AmB (Sigma no. A2942) for *Li*AmB1000.1, and 200 μM MF (Cayman Chem no. 63280) for *Li*MF200.5.

Anti-Leishmanial Activity Assay. Antileishmanial activity was evaluated in *Leishmania* promastigotes by monitoring parasite proliferation over 72 h of incubation at 25 °C. In the presence of increasing concentrations of the tested compound, parasite growth was quantified by measuring absorbance at 600 nm (A600) on a Cytation 5 plate reader (BioTek-Agilent, Santa Clara, CA, USA). The EC_{50} values—defined as the concentration required to reduce parasite growth by 50%—were calculated from dose−response curves using nonlinear regression and the GraphPad Prism 10.0 program (GraphPad Software, La Jolla, CA, USA). Each assay was performed in triplicate with three independent biological replicates conducted for each compound.

Evaluation of Drug Susceptibility in Leishmania-Infected Macrophages. As previously described to determine effective concentration (EC_{50}) values,[44] bone-marrow-derived macrophages (BMDMs, 2.5 × 10^5) were seeded in 12-well chamber slides containing complete DMEM medium. Stationary-phase *L. infantum* promastigotes were added at a 1:5 macrophage-to-parasite ratio for infection. The infected cells were incubated for 4 h at 37 °C in an environment containing 5% CO_2 without an additional drug. After 24 h, increasing concentrations of propargyl ether **20** (0, 5, 25, 50, 100, and 300 nM) were introduced to the infected macrophages. After 48 h, the infected cultures were subjected to methanol fixation and stained with Diff-Quick for parasite visualization. The number of intracellular amastigotes per 100 cells was quantified by examining 300 macrophages per triplicate assay and normalized to the untreated control. The median EC_{50} values were calculated from dose−response curves that were analyzed by nonlinear regression using GraphPad Prism 10.0. The data presented herein reflect the mean of three independent biological replicates.

Primary Bone-Marrow-Derived Macrophage (BMDM). Cells were collected from the tibia and femurs of 8−12 wk-old C57BL/6 female mice (Charles River Laboratory) and cultured in full medium [DMEM (Wisent) containing 10% heat-inactivated FBS, antibiotics, and 20% L cell−conditioned medium (LCCM)] as a source of macrophage CSF. After 4 days, the cells were supplemented with 10% LCCM. On day 7, cells were harvested by gentle washing of the monolayer with PBS-EDTA. After centrifugation, cells were counted and frozen in freezing medium [50% FBS, 10% DMSO, and 40% full medium (DEMEM/FBS/LCCM/PS)].

Cytotoxicity Assay in Mammalian Cell Lines. It was performed with BMDM cells, which were seeded at 5 × 10^4 cells/well in 96-well plates and preincubated in a 95% air-humidified atmosphere and 5% CO_2 for 24 h at 37 °C. After 24 h, the medium was replaced with 100 μL of fresh medium containing a 2-fold serial dilution concentration of the tested compound at different concentrations (50−0.019 μM) and kept in the incubator for another 24 h. As a negative control, DMSO at 0.5% was used (solvent control). After incubation, a new medium replacement was performed with the addition of 100 μL of fresh medium containing 10% of Alamar blue (Invitrogen). The plates were incubated at 37 °C under 5% CO2 and 95% humidity for 4 h. Absorbance was measured at two wavelengths (570 and 600 nm) and analyzed according to the manufacturer's protocol. The cytotoxicity results were normalized by vehicle (0.5% DMSO), and the CC_{50} was calculated based on dose−response curves analyzed by nonlinear regression with GraphPad Prism 10.0 software. All experiments were performed in triplicate, and data are represented as the mean of three samples with a standard deviation.

Anti-T. cruzi Activity. It was measured using the epimastigote forms of *T. cruzi* strain Basileu, which were grown in LIT medium supplemented with 10% fetal bovine serum and 10 μg/mL of hemein at 25 °C with two passages per week. Anti-*T. cruzi* activity was measured based on the replication of 1 × 10^6 epimastigote forms of *T. cruzi* strain Basileu incubated at 25 °C in the presence of increasing concentrations of the different compounds after 72 h. After the incubation, absorbance was measured at 600 nm, and EC_{50} values were calculated based on the dose−response curves analyzed by nonlinear regression with GraphPad Prism 10.0 software (GraphPad Software, La Jolla, CA, USA). All experiments were performed in triplicate, and data are represented as the mean of three samples with standard deviation.

Anti-Trypanosoma brucei Activity. It was performed using the procyclic form of *T. brucei*, which was grown in SDM medium supplemented with 10% fetal bovine serum and 5 μg/mL of hemein at 25 °C by two passages per week. Anti-*T. brucei* activity was measured based on the replication of 1 × 10^6 procyclic forms of *T. brucei* incubated at 25 °C in the presence of increasing concentrations of the different compounds after 72 h. After the incubation, absorbance was measured at 600 nm, and EC_{50} values were calculated based on dose−response curves analyzed by nonlinear regression with GraphPad Prism 10.0 software (GraphPad Software, La Jolla, CA, USA). All experiments were performed in triplicate, and data are represented as the mean of three samples with standard deviation.

https://doi.org/10.1021/acs.jmedchem.5c01291
J. Med. Chem. 2025, 68, 20264−20282

Purification of 80S Ribosomes for Cryo-EM. Mid log phase *L major* strain Friedlin (LM14Cs1H3 sKO) cells[53] ($1.5-2 \times 10^7$ cells/ml, ~1 g pellet) were washed three times in resuspension buffer (45 mM HEPES-KOH pH 7.6, 100 mM KOAc, 10 mM $Mg(OAc)_2$, and 250 mM Sucrose) and then suspended in cold buffer-A (45 mM HEPES-KOH pH 7.6, 100 mM K(OAc), 10 mM $Mg(OAc)_2$, 250 mM Sucrose, 5 mM β-mercaptoethanol, and a 1:40 dilution of Rnasin U (Promega). Cells were lysed using nitrogen cavitation (750 psi N_2, 45 min, 4 °C). Cell debris was removed by centrifugation (30 min at 9000 rpm) at 4 °C. The lysate was gently loaded onto a 1.1 M sucrose cushion in cold buffer-B (20 mM HEPES-KOH pH 7.6, 150 mM KOAc, 10 mM $Mg(OAc)_2$, 1.1 M sucrose, and 5 mM β-mercaptoethanol) and centrifuged at 55,000 rpm at 4 °C for 15 h (Ti70 rotor, Beckman). Upon centrifugation, the pellet was resuspended in cold buffer-C (20 mM HEPES-KOH pH 7.6, 150 mM KOAc, 10 mM $Mg(OAc)_2$, and 5 mM β-mercaptoethanol) and loaded onto a 10−40% (w/v) sucrose gradient in buffer-C for centrifugation (22,000 rpm, 11 h, on SW28 rotor, Beckman). The peak corresponding to 80S ribosomes was collected, balanced with buffer-C, and centrifuged at 55,000 rpm for 12 h at 4 °C. The resulting pellet was suspended in buffer-D (20 mM HEPES-KOH, pH 7.6, 100 mM KOAc, 10 mM $Mg(OAc)_2$, 10 mM NH_4OAc, and 1 mM DTT) and centrifuged for 90 min at 75,000 rpm (TLA-100 rotor, Beckman). The final ribosome pellet was gently resuspended in buffer-D, and aliquots were flash-frozen and stored at −80 °C until further use. The identity of 80S was further confirmed by mass-spectrometric analysis.

*Ternary 80S Complex Formation with mRNA, tRNA, and Ether **20**.* To reconstitute the classical-PRE-ribosome complex with mRNA and tRNA molecules, vacant 80S ribosomes were sequentially mixed with mRNA fragment coding for methionine (AUG) and phenylalanine (UUC) codons (CACCAUGUUCAAA, Integrated DNA Technologies, Inc.), a P-site $tRNA^{fMet}$ (*E. coli*, Sigma), and an A-site $tRNA^{Phe}$ (*E. coli*, Sigma) at a 1:100:5:5 stoichiometric ratio.[53] Subsequently, ether **20** (20 μM) was added. The complex assembly was performed at 37 °C in buffer-D (20 mM HEPES-KOH, pH 7.6, 100 mM KOAc, 10 mM $Mg(OAc)_2$, 10 mM NH_4OAc, and 1 mM DTT) with a relaxation time of 15 min after the addition of each component.

Cryo-EM Data Collection and Refinement. To prepare cryo-EM grids, 3.5 μL of ribosome suspension (~12A of A_{260}) was applied to glow-discharged holey carbon grids (Quantifoil R2/2) coated with a continuous thin carbon film. The grids were blotted and plunge-frozen using Vitrobot Mark IV (Thermo Fischer Scientific). A Titan Krios electron microscope (Thermo Fischer Scientific) operating at 300 kV equipped with a K3 direct electron detector (Gatan Inc.) was used for collecting cryo-EM micrographs at liquid nitrogen temperature at a nominal magnification of 105,000×, with a pixel size of 0.8245 Å/pixel and a dose rate of ~0.9269 electron/Å^2/frame. Defocus values ranged from −0.5 to −1.5 μm. Relion 3.1 and Relion 5.0 were used for data processing.[76] Motion correction and contrast transfer function parameters were estimated using Motioncor2[77] and CTFFIND-3,[78] respectively. The extracted particles were subjected to several rounds of unsupervised 3D classification using a low-pass filtered cryo-EM density map. 3D classes similar to 80S particles were selected and subjected to autorefinement in Relion 3.1 and Relion 5.0. Upon initial refinement, particles were subjected to CTF refinement, Bayesian polishing, and refinement. The resulting high-resolution 3D density map was then subjected to a cycle of multibody refinement using separate masks for the large subunit, as well as the head and body regions of the small subunit (SSU).[79] The gold standard Fourier shell correlation value criterion of 0.143 was used for determining averaged map resolutions, as implemented in Relion 3.1 and Relion 5.0.

Model Building and Refinement. rRNA and rProtein models were built by template-guided model building in COOT.[80] The coordinates of the *L. major* ribosome (PDB ID: 8RXH) were used as a template for model building and were docked onto density maps using UCSF ChimeraX.[81] The Mg^{2+}, Zn^{2+}, Na^+, and K^+ ion compositions were modeled according to the recently described criteria.[54,82] Model refinement was performed using an iterative approach, including real-space refinement and geometry regularization in COOT,[80] followed by real-space refinement using the PHENIX suite.[83] The final model was validated using MolProbity.[84] Ligand-rRNA interactions were calculated using LigPlot+.[85]

Thermal Proteome Profiling. For TPP analysis, *L. infantum* promastigotes were prepared.[56] Briefly, *L. infantum* wild-type (WT) cultures were centrifuged, and the resulting pellet was washed with 1× PBS (pH 7.4; Gibco, Life Technologies) before being resuspended in lysis buffer containing 50 mM monobasic potassium phosphate, 50 mM dibasic potassium phosphate, 0.5 M EDTA, 1 M DTT, 10 mM tosyl-L-lysyl-chloromethane hydrochloride, 0.8% *n*-octyl-β-D-glucoside, and a protease inhibitor cocktail (EDTA-free). After three freeze−thaw cycles and centrifugation, the lysate was collected. Drug-induced disruption and heat treatment were then performed on the lysate. The lysate was divided into subsamples treated with 100 μM anisomycin (**7**), 100 μM *O*-propargyl ether **20**, or vehicle control (DMSO). For each condition, 250 μg of lysate was divided into seven microcentrifuge tubes, each incubated at a different temperature (37, 45, 50, 55, 60, 65, or 70 °C) for 3 min. Following incubation, the soluble protein fraction was collected by centrifugation. Proteins were alkylated and precipitated, and both the test samples and internal standards were labeled using a light and heavy dimethyl labeling strategy, respectively, for HPLC−MS/MS analysis. Data were analyzed using Thermo Proteome Discoverer and SEQUEST, with protein abundance normalized accordingly. Melting curves were subsequently generated in GraphPad Prism 10.0 (GraphPad Software, La Jolla, CA, USA) to determine the melting temperatures (T_m). The cutoff value for selecting candidate proteins was set at $\Delta T_m \geq 4$ °C.

Gene-Ontology (GO) Enrichment and Multiple-Testing Correction. All proteins quantified in the TPP experiment ($N = 2768$ and $N = 2503$) were used as the background for GO enrichment analysis. Proteins classified as "drug-responsive" ($|\Delta T_m| \geq 4$ °C) were analyzed independently after separation into three groups: common, anisomycin-specific, and ether **20**-specific. GO enrichment analysis was performed using the STRING database (version 12.0). Protein identifiers from each drug-responsive group were submitted to STRING, which returned associated GO biological-process terms, gene count, enrichment strength, and adjusted *P*-values (FDR). Functional annotation was based on the TriTrypDB, and only GO terms with both unadjusted $P < 0.05$ and Benjamini-adjusted $P < 0.05$ were retained.

GO enrichment results were visualized using R (version 4.3.2) with the *ggplot2* and *ggpubr* packages. For the full enrichment output, the 30 most significant GO biological-process terms were selected based on their −log10-transformed FDR values. Bubble plots were generated with *ggballoonplot*, with bubble size proportional to the number of drug-responsive proteins annotated to each term and color intensity representing the statistical significance (−log10-transformed FDR), according to the scale shown in the figure legend.

*Chemistry. tert-Butyl (2R,3S,4S)-3-acetoxy-4-hydroxy-2-(p-hydroxybenzyl)pyrrolidine-1-carboxylate (**13**).* *N*-(Boc)-Desmethylanisomycin (**13**) was prepared by employing a modification of the literature protocol.[44] A 25 mL round-bottomed flask containing a 10 mm × 5 mm polytetrafluoroethylene-coated magnetic stir bar was flame-dried and cooled under argon from a 20-gauge needle fitted with an inflated balloon. The flask was charged with anisomycin (**7**, 100 mg, 0.377 mmol, 100 mol %), flushed with argon, and treated with DCM (6.28 mL). The homogeneous solution was cooled to −78 °C, treated by a syringe (50 μL Hamilton glass syringe) over 10 min with a solution of BBr_3 (142 mg, 0.565 mmol, 150 mol %), and stirred for 5 min. The cooling bath was removed. Stirring was continued for 30 min when a white turbid mixture was observed, and mass spectrometric analysis showed the disappearance of the molecular ion corresponding to methyl ether **7** and the appearance of an ion for the corresponding phenol. After cooling in an ice bath, the mixture was treated slowly with saturated aqueous sodium bicarbonate until the pH was 8−9. Di-*tert*-butyl-bicarbonate (Boc_2O, 90.5 mg, 0.415 mmol, 110 mol %) was added to the biphasic mixture, which was stirred vigorously for 1 h when TLC showed a less polar product [$R_f = 0.64$ (80% EtOAc in hexanes)] and mass spectrometric analysis showed disappearance of the molecular ion corresponding to the amine and appearance of an ion for corresponding carbamate **13**. The volatiles were evaporated, and the

https://doi.org/10.1021/acs.jmedchem.5c01291
J. Med. Chem. 2025, 68, 20264−20282

residue was partitioned between EtOAc (10 mL) and water (5 mL). The organic layer was separated, dried over Na_2SO_4, filtered, and evaporated to a residue, which was purified by flash chromatography (on a 30 cm × 2.5 cm fritted disk column containing 35 g of silica gel) eluting with a gradient of 50−90% of EtOAc in hexanes. Evaporation of the collected fractions under reduced pressure (bath temperature 40 °C) afforded *N*-Boc-desmethylanisomycin (**13**, 130 mg, 98%) as a white solid: R_f = 0.64 (20% hexanes in EtOAc); LC−MS analysis (λ = 214 nm) RT = 9.26 min, >99% purity, using 10−90% MeOH (0.1% FA) in water (0.1% FA) over 14 min; m/z = 374.1 $[M + Na]^+$. ^{1}H NMR (400 MHz, $CDCl_3$): δ 6.94 (d, J = 8.7 Hz, 2H), 6.73 (d, J = 7.2 Hz, 2H), 4.86 (t, J = 5.9 Hz, 1H), 4.35 (q, J = 6.3 Hz, 1H), 3.9 (br s, 1H), 3.49−3.26 (m, 3H), 2.78 (s, 2H), 2.06 (s, 3H), 1.45 (s, 9H). $^{13}C\{^1H\}$ NMR (100 MHz, $CDCl_3$): δ 171.2, 155.0, 146.8, 130.6, 129.0, 115.6, 85.3, 80.8, 79.0, 71.2, 58.8, 28.5, 27.5, 21.0. HRMS (ESI^+) calcd m/z for $C_{18}H_{25}NO_6Na$ $[M + Na]^+$ 374.1574; found, 374.1572.

*tert-Butyl (2R,3S,4S)-3-acetoxy-2-(4-(2-(benzyloxy)-2-oxoethoxy)benzyl)-4-hydroxypyrrolidine-1-carboxylate (**14**).* A flame-dried 5 mL round-bottom flask under a nitrogen atmosphere was charged with carbamate **13** (30 mg, 0.084 mmol, 100 mol %), which was dissolved in dry DMF (0.54 mL, 155 mM), treated with Cs_2CO_3 (33.4 mg, 0.102 mmol, 120 mol %), stirred for 5 min, treated with a 0.44 M solution of benzyl bromoacetate in DMF (0.24 mL, 0.103 mmol, 120 mol %), heated at 65 °C, and stirred for 3 h, until TLC showed disappearance of starting material and appearance of a less polar spot corresponding to benzyl ester **14** [R_f = 0.28 (30% EtOAc in hexanes)]. The reaction mixture was transferred to a Falcon 15 mL conical centrifuge tube and partitioned between EtOAc (5 mL) and water (5 mL), and the organic phase was washed with water (5 mL). The combined aqueous layer was back-extracted with EtOAc (2 × 5 mL). The combined organic layer was washed with brine (3 mL), dried over Na_2SO_4, filtered, and evaporated to a residue which was purified by flash chromatography (on a 30 cm × 1.5 cm fritted disc column containing 15.4 g of silica gel) eluting with a gradient of 10−60% of EtOAc in hexanes. Evaporation of the collected fractions under reduced pressure (bath temperature 40 °C) afforded ester **14** (34.1 mg, 80%) as a viscous colorless oil: R_f = 0.28 (30% EtOAc in hexanes): LC−MS analysis (λ = 214 nm), RT = 9.30 min, >99% purity, using 10−90% MeCN (0.1% FA) in water (0.1% FA) over 14 min; m/z = 522.2 $[M + Na]^+$. ^{1}H NMR (400 MHz, $CDCl_3$): δ 7.36−7.33 (m, 5H), 7.06 (d, J = 6.6 Hz, 2H), 6.79 (d, J = 8.7 Hz, 2H), 5.23 (s, 2H), 4.87 (t, J = 6.0 Hz, 1H), 4.62 (s, 2H), 4.37 (m, 1H), 4.01 (m, 1H), 3.46 (m, 1H), 3.33 (m, 1H), 3.07−2.72 (m, 3H), 2.06 (s, 3H), 1.45 (s, 9H). $^{13}C\{^1H\}$ NMR (100 MHz, $CDCl_3$): δ 171.0, 169.0, 156.5, 154.6, 135.3, 131.4, 130.6, 128.8, 128.7, 128.6, 114.8, 80.2, 80.2, 79.3, 71.8, 67.1, 65.6, 58.9, 29.8, 28.6, 21.0. HRMS (ESI^+) calcd m/z for $C_{27}H_{33}NO_8Na$ $[M + Na]^+$ 522.2098; found, 522.2084.

*HCC(CH$_2$)$_4$CO-Val(Me)-Val-Val-Ala-Phe-NH(CH$_2$)$_6$NH−CO−CH$_2$−anisomycin (**18**).* A flame-dried 10 mL round-bottom flask with a 10 mm × 4 mm magnetic stir bar under an argon atmosphere was charged with benzyl ester **14** (41.9 mg, 83.9 μmol, 100 mol %), which was dissolved in MeOH (4.93 mL, 17 mM), and treated with Pd/C (4.19 mg, 10 wt %). The flask was purged thrice with argon. After stirring for 30 min, the mixture was placed under a balloon of hydrogen and stirred for 1 h, when TLC with staining using bromocresol green indicated the complete removal of the benzyl protection. The reaction mixture was filtered through Celite. The filtrate was evaporated to give *O*-carboxymethyl anisomycin **15**, which was used without further purification. A solution of MeVal[1]-almiramide **11** (34 mg, 0.044 mmol, 100 mol %)[46] in dry CH_2Cl_2 (15 mL) was treated with acid **15** (21.7 mg, 0.053 mmol, 120 mol %), DCC (10.9 mg, 0.053 mmol, 120 mol %), and HOBt (7.15 mg, 0.053 mmol, 120 mol %), stirred for 48 h, and filtered through Celite. The filter cake was washed with CH_2Cl_2. The filtrate and washings were evaporated under reduced pressure. The residue was purified by HPLC on a C18 column using a gradient of 30% to 90% MeOH (0.1% FA) in H_2O (0.1% FA). Evaporation of the collected fractions afforded a white solid (29 mg, 6% yield [RT 10.4 min, 50−90% MeOH (0.1% FA) in H_2O (0.1% FA) over 14 min), which was dissolved in DCM (5 mL) and treated with HCl gas bubbles for 1 h. Evaporation of the volatiles under reduced pressure gave conjugate **18** (20.4 mg, 44%): LC−MS analysis (λ = 280 nm) RT 7.77 min, >99% purity, using 10−90% MeOH (0.1% FA) in H_2O (0.1% FA), over 14 min]. HRMS (ESI^+) calcd m/z for $C_{56}H_{85}N_8O_{11}$ $[M + H]^+$ 1045.6332; found, 1045.6339.

*HCC(CH$_2$)$_4$CO-Val-Val-Val-Ala-Phe(Me)-NH(CH$_2$)$_6$NH−CO−CH$_2$−anisomycin (**19**).* A solution of Phe(Me)[5]-almiramide **12**[46] (34 mg, 0.044 mmol, 100 mol %) in dry CH_2Cl_2 (15 mL) was treated with acid **15** (21.7 mg, 0.053 mmol, 120 mol %), DCC (10.9 mg, 0.053 mmol, 120 mol %), and HOBt (7.15 mg, 0.053 mmol, 120 mol %) and stirred for 48 h and filtered through Celite. The filter cake was washed with CH_2Cl_2. The filtrate and washings were evaporated under reduced pressure. The residue was purified by HPLC on a C18 column using a gradient of 30% to 90% MeOH (0.1% FA) in H_2O (0.1% FA). Evaporation of the collected fractions afforded a white solid {32 mg, 7% yield [RT 10.47 min, 50−90% MeOH (0.1% FA) in H_2O (0.1% FA)] over 14 min}, which was dissolved in DCM (5 mL) and treated with HCl gas bubbles for 1 h. Evaporation of the volatiles under reduced pressure gave conjugate **19** (17.8 mg, 39%): LC−MS analysis (λ = 280 nm) RT 7.82 min, >99% purity, using 10−90% MeOH (0.1% FA) in H_2O (0.1% FA), over 14 min]. HRMS (ESI^+) calcd m/z for $C_{56}H_{85}N_8O_{11}$ $[M + H]^+$ 1045.6332; found, 1045.6341.

*(2R,3S,4S)-4-Hydroxy-2-(4-(prop-2-yn-1-yloxy)benzyl)pyrrolidin-3-yl Acetate Hydrochloride (**20**).* A flame-dried 10 mL round-bottom flask under an inert N_2 atmosphere was charged with *N*-Boc-desmethylanisomycin (**13**, 37.9 mg, 0.108 mmol, 100 mol %) in dry DMF (5.39 mL, 20 mM). The solution was treated with Cs_2CO_3 (42.2 mg, 0.129 mmol, 120 mol %), stirred for 5 min, treated with propargyl bromide (80 wt % in toluene, 11.6 μL, 0.129 mmol, 120 mol %), heated at 65 °C, and stirred for 2 h, when TLC showed disappearance of phenol **13** and appearance of a less polar spot corresponding to *N*-Boc-*O*-propargyl ether [R_f = 0.17, 30% EtOAc in hexanes]. The reaction mixture was transferred to a 30 mL separating funnel and partitioned between EtOAc (12 mL) and water (12 mL). The aqueous layer was extracted with EtOAc (2 × 12 mL). The combined organic layer was washed with brine (12 mL), dried over Na_2SO_4, filtered, and evaporated to a residue, which was purified by flash chromatography (on a 30 × 1.5 cm fritted disk column containing 15.0 g of silica gel) eluting with a gradient of 10−50% of EtOAc in hexanes. Evaporation of the collected fractions under reduced pressure (bath temperature 40 °C) afforded a viscous colorless oil (28.7 mg, 68% yield): ^{1}H NMR (400 MHz, $CDCl_3$): δ 7.08 (d, J = 7.7 Hz, 2H), 6.88 (d, J = 8.9 Hz, 2H), 4.89 (t, J = 6.2 Hz, 1H), 4.66 (d, J = 2.4 Hz, 2H), 4.41−4.36 (m, 1H), 4.03 (m, 1H), 3.48 (m, 1H), 3.35 (m, 1H), 2.99 (m, 1H), 2.87−2.81 (m, 1H), 2.54−2.50 (overlapping m and t, J = 2.4 Hz, 2H), 2.08 (s, 3H), 1.46 (s, 9H). The oil was dissolved in dry DCM (3.68 mL, 20 mM) and treated with HCl gas bubbles for 30 min when TLC showed the disappearance of the starting material and appearance of a ninhydrin and $KMnO_4$ active baseline spot (30% EtOAc in hexanes). Evaporation of the volatiles on a rotary evaporator equipped with a trap containing saturated $NaHCO_3$ gave the *O*-propargyl ether hydrochloride **20** as a white solid (16.8 mg, 70%): LC−MS analysis (λ = 214 nm), >99% purity [RT 3.61 min, 10−90% MeOH (0.1% FA) in H_2O (0.1% FA); RT 5.16 min, 5−50% MeCN (0.1% FA) in H_2O (0.1% FA), over 14 min, respectively]. ^{1}H NMR (400 MHz, D_2O): δ 7.29 (d, J = 8.7 Hz, 2H), 7.07 (d, J = 8.7 Hz, 2H), 5.12 (d, J = 3.2 Hz, 1H), 4.80 (d, J = 2.4 Hz, 2H), 4.49 (br d, J = 4.9 Hz, 1H), 4.28 (td, J = 8.8, 3.6 Hz, 1H), 3.72 (dd, J = 13.5, 5.0 Hz, 1H), 3.29 (d, J = 13.5 Hz, 1H), 3.15 (dd, J = 14.3, 7.2 Hz, 1H), 3.08 (dd, J = 14.1, 8.6 Hz, 1H), 2.95 (t, J = 2.4 Hz, 1H), 2.21 (s, 3H); $^{13}C\{^1H\}$ NMR (100 MHz, D_2O): δ 172.2, 156.0, 130.0, 129.1, 115.7, 78.7, 76.9, 76.7, 72.0, 61.9, 56.0, 50.8, 30.4, 20.1. HRMS (ESI^+) calcd m/z for $C_{16}H_{20}NO_4$ $[M + H]^+$ 290.1387; found, 290.1387.

*(2R,3S,4S)-4-Hydroxy-2-(4-(pent-4-yn-1-yloxy)benzyl)pyrrolidin-3-yl Acetate Hydrochloride (**21**).* Employing the protocol used for the preparation of ether **20**, *N*-Boc-desmethylanisomycin (**13**, 30.0 mg, 0.085 mmol, 100 mol %) in DMF (4.25 mL, 20.1 mM) was treated with Cs_2CO_3 (41.7 mg, 0.128 mmol, 150 mol %) and pent-4-yn-1-yl-4-methylbenzenesulfonate (22.4 mg, 0.0934 mmol, 110 mol %). After 75 min, TLC indicated the reaction completion. After aqueous workup, the *N*-Boc-*O*-pentynyl ether [R_f = 0.53, 50% EtOAc in hexanes] was purified by flash chromatography (on a 30 cm × 1.5 cm fritted-disc

https://doi.org/10.1021/acs.jmedchem.5c01291
J. Med. Chem. 2025, 68, 20264−20282

column containing 15.5 g of silica gel) eluting with a gradient of 10−50% of EtOAc in hexanes. Evaporation of the collected fractions under reduced pressure (bath temperature 40 °C) afforded a viscous colorless oil (34.5 mg, 97% yield): ^{1}H NMR (400 MHz, $CDCl_3$): δ 7.06 (d, J = 7.0 Hz, 2H), 6.80 (d, J = 8.6 Hz, 2H), 4.89 (t, J = 6.1 Hz, 1H), 4.39 (m, 1H), 4.03−3.98 (overlapping m and t, J = 6.2 Hz, 3H), 3.48 (m, 1H), 3.33 (m, 1H), 3.04−2.85 (m, 2H), 2.40 (td, J = 7.1, 2.6 Hz, 2H), 2.10 (s, 3H), 2.01−1.96 (m, 3H), 1.46 (s, 9H).

The residue was dissolved in dry DCM (8.21 mL, 10.1 mM) and treated with HCl gas bubbles when a white precipitate formed. After 1 h, TLC showed the disappearance of the starting material and appearance of a ninhydrin and $KMnO_4$ active baseline spot (50% EtOAc in hexanes). The volatiles were evaporated. The residue was triturated with diethyl ether (2 × 5 mL) to provide *O*-pentyl ether hydrochloride **21** as a white solid (23 mg, 79%): LC−MS analysis (λ = 214 nm), >99% purity [RT 4.08 min, 10−90% MeOH (0.1% FA) in H_2O (0.1% FA), and RT 5.84 min, 10−90% MeCN (0.1% FA) in H_2O (0.1% FA), over 14 min, respectively]. ^{1}H NMR (400 MHz, CD_3OD): δ 7.22 (d, J = 8.5 Hz, 2H), 6.93 (d, J = 8.5 Hz, 2H), 5.07 (d, J = 3.2 Hz, 1H), 4.36 (br d, J = 4.4 Hz, 1H), 4.19−4.15 (m, 1H), 4.06 (t, J = 6.2 Hz, 2H), 3.59 (dd, J = 12.8, 4.6 Hz, 1H), 3.19 (d, J = 12.9 Hz, 1H), 3.09 (dd, J = 14.6, 6.7 Hz, 1H), 2.95 (dd, J = 14.3, 8.7 Hz, 1H), 2.37 (td, J = 7.0, 2.6 Hz, 2H), 2.24 (t, J = 2.6 Hz, 1H), 2.18 (s, 3H), 1.95 (quint, 2H); ^{13}C{^{1}H} NMR (100 MHz, CD_3OD): δ 170.8, 159.9, 131.0, 129.0, 116.2, 84.1, 78.3, 73.4, 70.0, 67.4, 63.7, 52.6, 32.2, 29.4, 20.6, 15.7. LCMS (ESI+) m/z for $C_{18}H_{23}NO_4$ [M + H]$^+$ 318.1. HRMS (ESI$^+$) calcd m/z for $C_{18}H_{24}NO_4$ [M + H]$^+$ 318.1699; found, 318.1695.

*(2R,3S,4S)-2-(4-(Hex-5-yn-1-yloxy)benzyl)-4-hydroxypyrrolidin-3-yl Acetate Hydrochloride (**22**).* Employing the protocol used for the preparation of ether **20**, using *N*-Boc-desmethylanisomycin (**13**, 50.0 mg, 0.142 mmol, 100 mol %) in dry DMF (1.7 mL, 83.7 mM), Cs_2CO_3 (55.6 mg, 0.171 mmol, 120 mol %) and hex-5-yn-1-yl-4-methylbenzenesulfonate (43.1 mg, 0.171 mmol, 120 mol %) were treated. After aqueous workup, the *N*-Boc-*O*-hexynyl ether [R_f = 0.55, 50% EtOAc in hexanes] was purified by flash chromatography (on a 30 cm × 1.5 cm fritted-disc column containing 15.3 g of silica gel), eluting with a gradient of 10−30% EtOAc in hexanes. Evaporation of the collected fractions under reduced pressure (bath temperature 40 °C) afforded as a viscous colorless oil (34.1 mg, 56% yield): ^{1}H NMR (400 MHz, $CDCl_3$): δ 7.04 (d, J = 8.0 Hz, 2H), 6.78 (d, J = 8.7 Hz, 2H), 4.88 (t, J = 6.2 Hz, 1H), 4.39−4.35 (m, 1H), 4.00−3.94 (overlapping m and t, J = 6.3 Hz, 3H), 3.46 (m, 1H), 3.3 (m, 1H), 3.05−2.79 (m, 3H), 2.26 (td, J = 7.1, 2.6 Hz, 2H), 2.08 (s, 3H), 1.96 (t, J = 2.6 Hz,1H), 1.92−1.85 (m, 2H), 1.74−1.67 (m, 2H), 1.45 (s, 9H).

The residue was dissolved in dry DCM (3.95 mL, 20 mM) and treated with HCl gas bubbles when a white precipitate formed. After 30 min, TLC showed the disappearance of the starting material and the appearance of a ninhydrin and $KMnO_4$ active baseline spot (50% EtOAc in hexane). The volatiles were evaporated. The residue was triturated with diethyl ether (2 × 5 mL). Analysis by LC−MS (l = 214 nm, 10−90% MeOH (0.1% FA) in water (0.1% FA), over 14 min) showed the triturated residue (RT = 7.05 min; m/z = 332.2 [M + H] $^+$) to be of 90% purity contaminated with product having a molecular ion corresponding to the desmethylanisomycin (10%, RT = 2.43 min, m/z = 252.1 [M + H] $^+$). Purification by reverse-phase HPLC on a Waters C18 column (SunFire, particle size, 10 μm, 150 mm × 10 mm) and evaporation of the collected fractions gave *O*-hexynyl ether **22** as a white solid (20 mg, 69%): LC−MS analysis (λ = 214 nm), >99% purity [RT 6.82, 10−90% MeOH (0.1% FA) in H_2O (0.1% FA), and RT 5.99 min, 10−90% MeCN (0.1% FA) in H_2O (0.1% FA), over 14 min, respectively]. ^{1}H NMR (400 MHz, D_2O): δ 8.45 (s, 1H), 7.26 (d, J = 8.7 Hz, 2H), 7.01 (d, J = 8.7 Hz, 2H), 5.09 (d, J = 3.1 Hz, 1H), 4.47 (br d, J = 4.7 Hz, 1H), 4.25 (td, J = 8.6, 3.5 Hz, 1H), 4.10 (t, J = 6.4 Hz, 2H), 3.69 (dd, J = 13.1, 4.8 Hz, 1H), 3.26 (d, J = 13.3 Hz, 1H), 3.13 (dd, J = 14.2, 7.2 Hz, 1H), 3.07 (dd, J = 14.5, 8.9 Hz, 1H), 2.35 (t, J = 2.7 Hz, 1H), 2.28 (td, J = 6.9, 2.5 Hz, 2H), 2.21 (s, 3H), 1.91−1.84 (m, 2H), 1.72−1.64 (m, 2H); ^{13}C{^{1}H} NMR (100 MHz, D_2O): δ 172.2, 157.4, 130.0, 128.4, 115.4, 85.8, 77.0, 72.1, 69.3, 68.1, 61.9, 50.8, 30.5, 27.5, 24.3, 20.1, 17.3. HRMS (ESI$^+$) calcd m/z for $C_{19}H_{26}NO_4$ [M + H]$^+$ 332.1856; found, 332.1868.

*(2R,3S,4S)-2-(4-(Hept-6-yn-1-yloxy)benzyl)-4-hydroxypyrrolidin-3-yl Acetate Hydrochloride (**23**).* Employing the protocol used for the preparation of ether **20**, using *N*-Boc-desmethylanisomycin (**13**, 30.4 mg, 0.0865 mmol, 100 mol %) in dry DMF (0.7 mL, 124 mM), Cs_2CO_3 (33.8 mg, 0.104 mmol, 120 mol %) and hept-6-yn-1-yl-4-methylbenzenesulfonate (26.0 mg, 0.0978 mmol, 110 mol %) were added. After heating at 74 °C for 3 h, TLC indicated a complete reaction. After aqueous workup, the *N*-Boc-*O*-heptynyl ether [R_f = 0.56, 50% EtOAc in hexanes] was purified by flash chromatography (on a 30 cm × 1.5 cm fritted-disc column containing 15.8 g of silica gel) eluting with a gradient of 10−30% EtOAc in hexanes. Evaporation of the collected fractions under reduced pressure (bath temperature 40 °C) afforded a viscous colorless oil (25.4 mg, 66% yield): ^{1}H NMR (400 MHz, $CDCl_3$): δ 7.05 (d, J = 8.2 Hz, 2H), 6.79 (d, J = 8.6 Hz, 2H), 4.88 (t, J = 6.2 Hz, 1H), 4.41−4.36 (m, 1H), 4.02−3.97 (m, 1H), 3.93 (t, J = 6.4 Hz, 2H), 3.48 (m, 1H), 3.33 (m, 1H), 3.02−2.85 (m, 3H), 2.24−2.21 (m, 2H), 2.10 (s, 3H), 1.95 (t, J = 2.6 Hz, 1H), 1.82−1.75 (m, 2H), 1.62−1.57 (m, 2H), 1.46 (s, 9H), 1.25 (m, 2H).

The residue was dissolved in dry DCM (2.00 mL, 26.3 mM) and treated with HCl gas bubbles when a white precipitate formed. After 60 min, TLC showed the disappearance of the starting material and the appearance of a ninhydrin and $KMnO_4$ active baseline spot (50% EtOAc in hexane). The volatiles were evaporated. The residue was triturated with diethyl ether (2 × 5 mL). Analysis by LC−MS [λ = 254 nm, 10−90% MeOH (0.1% FA) in water (0.1% FA), over 14 min] showed the triturated residue (RT = 5.08 min; m/z = [M + H]$^+$ = 346.2) to be of 90% purity contaminated with product having a molecular ion corresponding the desacetyl anisomycin (10%, RT = 4.77 min; m/z = 304.2 [M + H]$^+$). Purification of 23.4 mg of the residue by reverse-phase HPLC on a Waters C18 column (SunFire, particle size, 10 μm, 150 × 10 mm) and evaporation of the collected fractions gave *O*-heptynyl ether **23** as a white solid (10.9 mg, 54%): LC−MS analysis (λ = 214 nm), >99% purity [RT 7.44, 10−90% MeOH (0.1% FA) in H_2O (0.1% FA), and RT 6.19 min, 10−90% MeCN (0.1% FA) in H_2O (0.1% FA), over 14 min, respectively]. ^{1}H NMR (400 MHz, CD_3OD): δ 8.54 (br s, 1H), 7.20 (d, J = 8.5 Hz, 2H), 6.91 (d, J = 8.7 Hz, 2H), 5.05 (d, J = 2.3 Hz, 1H), 4.34 (br d, J = 4.3 Hz, 1H), 4.16−4.11 (m, 1H), 3.96 (t, J = 6.2 Hz, 2H), 3.58 (dd, J = 12.7, 4.6 Hz, 1H), 3.18 (d, J = 12.7 Hz, 1H), 3.06 (dd, J = 14.2, 6.9 Hz, 1H), 2.95 (dd, J = 14.2, 8.7 Hz, 1H), 2.22−2.18 (m, 3H), 2.17 (s, 3H), 1.82−1.75 (m, 2H), 1.62- 1.54 (m, 4H); ^{13}C{^{1}H} NMR (100 MHz, CD_3OD): δ 170.8, 160.0, 131.0, 129.0, 116.1, 84.9, 78.4, 73.5, 69.6, 68.9, 63.5, 52.6, 32.3, 29.9, 29.5, 26.3, 20.6, 19.0. HRMS (ESI$^+$) calcd m/z for $C_{20}H_{28}NO_4$ [M + H]$^+$ 346.2013; found, 346.2009.

*(2R,3S,4S)-4-Hydroxy-2-(4-(oct-7-yn-1-yloxy)benzyl)pyrrolidin-3-yl Acetate (**24**).* Employing the protocol used for the preparation of ether **20**, *N*-Boc-desmethylanisomycin (**13**, 20.0 mg, 0.0569 mmol, 100 mol %) in dry DMF (0.45 mL, 126 mM) was treated with Cs_2CO_3 (22.3 mg, 0.0683 mmol, 120 mol %) and oct-7-yn-1-yl-4-methylbenzenesulfonate (19.1 mg, 0.0683 mmol, 120 mol %). After the sample was heated at 65 °C for 2 h, TLC indicated complete reaction. After aqueous workup, the *N*-Boc-*O*-octynyl ether [R_f = 0.6, 50% EtOAc in hexanes] was purified by flash chromatography (on a 30 cm × 1.5 cm fritted-disc column containing 15.4 g of silica gel) eluting with a gradient of 10−30% EtOAc in hexanes. Evaporation of the collected fractions under reduced pressure (bath temperature 40 °C) afforded a viscous colorless oil (17 mg, 65% yield): ^{1}H NMR (400 MHz, $CDCl_3$): δ 7.04 (d, J = 7.3 Hz, 2H), 6.78 (d, J = 8.4 Hz, 2H), 4.88 (t, J = 5.9 Hz, 1H), 4.37 (m, 1H), 4.00 (m, 1H), 3.91 (t, J = 6.3 Hz, 2H), 3.46 (m, 1H), 3.33 (m, 1H), 3.02−2.80 (m, 2H), 2.62 (m, 1H), 2.20 (td, J = 6.7, 2.3 Hz, 2H), 2.08 (s, 3H), 1.94 (t, J = 2.3 Hz, 1H), 1.80−1.75 (m, 2H), 1.61−1.54 (m, 2H), 1.46 (overlapping m and s, 11H), 1.25 (br s, 2H).

The residue was dissolved in dry DCM (4.55 mL, 8.46 mM) and treated with HCl gas bubbles. After 4 h, TLC showed the disappearance of the starting material and appearance of a ninhydrin and $KMnO_4$ active baseline spot (50% EtOAc in hexanes). The volatiles were evaporated. The residue was precipitated with diethyl ether (2 × 5 mL) and centrifuged to provide the desired *O*-octynyl ether hydrochloride **24** as a white solid (13.8 mg, 91%): LC−MS analysis (λ = 214 nm), >99% purity [RT 5.50 min, 10−90% MeOH (0.1% FA) in H_2O (0.1%

https://doi.org/10.1021/acs.jmedchem.5c01291
J. Med. Chem. 2025, 68, 20264−20282

FA), and RT 6.34 min, 10−90% MeCN (0.1% FA) in H_2O (0.1% FA), over 14 min, respectively]. ^{1}H NMR (400 MHz, D_2O): δ 7.19 (d, J = 7.7 Hz, 2H), 6.88 (d, J = 8.6 Hz, 2H), 4.98 (d, J = 3.3 Hz, 1H), 4.46 (br d, J = 4.7 Hz, 1H), 4.22 (td, J = 8.2, 3.4 Hz, 1H), 3.92 (t, J = 6.5 Hz, 2H), 3.71 (dd, J = 13.3, 4.5 Hz, 1H), 3.31 (d, J = 13.6 Hz, 1H), 3.12−3.02 (m, 2H), 2.26 (t, J = 2.4 Hz, 1H), 2.17 (s, 3H), 2.16−2.14 (m, 2H) 1.73−1.66 (m, 2H), 1.52- 1.45 (m, 2H), 1.41−1.39 (m, 4H). ; ^{13}C{^{1}H} NMR (100 MHz, D_2O): δ 171.8, 157.6, 130.0, 127.9, 115.1, 85.7, 76.6, 71.9, 69.1, 68.3, 61.8, 51.0, 30.4, 28.4, 27.9, 27.8, 24.9, 20.2, 17.7. HRMS (ESI$^+$) calcd m/z for $C_{21}H_{30}NO_4$ [M + H]$^+$ 360.2169; found, 360.2163.

*(2R,3S,4S,2′RS)-2-(4-(Hex-5-yn-2′-yloxy)benzyl)-4-hydroxypyrrolidin-3-yl Acetate Hydrochloride (**25**).* Employing the protocol used for the preparation of ether **20**, *N*-Boc-desmethylanisomycin (**13**, 26.5 mg, 0.0754 mmol, 100 mol %) in dry DMF (0.6 mL, 126 mM) was treated with Cs_2CO_3 (29.5 mg, 0.0905 mmol, 120 mol %) and hex-5-yn-2′-yl-4-methylbenzenesulfonate (24.7 mg, 0.098 mmol, 130 mol %). After the mixture was heated at 70 °C for 3 h, TLC indicated complete reaction. After aqueous workup, the *N*-Boc-*O*-hex-5-yn-2′-yl ether [R_f = 0.7, 50% EtOAc in hexanes] was purified by flash chromatography (on a 30 cm × 1.5 cm fritted-disc column containing 15.2 g of silica gel) eluting with a gradient of 10−30% EtOAc in hexanes. Evaporation of the collected fractions under reduced pressure (bath temperature 40 °C) afforded a viscous colorless oil (19.7 mg, 61% yield): ^{1}H NMR (400 MHz, $CDCl_3$): δ 7.07 (d, J = 8.2 Hz, 2H), 6.80 (d, J = 8.5 Hz, 2H), 4.92 (t, J = 6.2 Hz, 1H), 4.53−4.45 (m, 1H), 4.43−4.39 (m, 1H), 4.07 (m, 1H), 3.51 (m, 1H), 3.36 (m, 1H), 3.03−2.83 (m, 2H), 2.51 (m, 1H), 2.37 (td, J = 6.9, 2.1 Hz, 2H), 2.11 (s, 3H), 2.00−1.91 (m, 2H), 1.85−1.77 (m, 1H), 1.48 (s, 9H), 1.32 (d, J = 5.9 Hz, 3H).

The residue was dissolved in dry DCM (5.40 mL, 8.46 mM) and treated with HCl gas bubbles when a white precipitate formed. After 4 h, TLC showed the disappearance of the starting material and appearance of a ninhydrin and $KMnO_4$ active baseline spot (50% EtOAc in hexanes). The volatiles were evaporated. The residue was precipitated with diethyl ether (2 × 5 mL) and centrifuged to provide the desired *O*-hex-5-yn-2′-yl ether hydrochloride **25** as a white solid (12.1 mg, 72%): LC−MS analysis (λ = 214 nm), >99% purity [RT 6.64 min, 10−90% MeOH (0.1% FA) in H_2O (0.1% FA), and RT 4.67 min, 10−90% MeCN (0.1% FA) in H_2O (0.1% FA), over 14 min, respectively]. ^{1}H NMR (400 MHz, D_2O): δ 7.27 (d, J = 8.8 Hz, 2H) (7.20 (d, J = 9 Hz, 0.13H)), 7.04 (d, J = 8.8 Hz, 2H) (6.9 (d, J = 8.14 Hz, 0.13H)), 5.10 (d, J = 3.3 Hz, 1H), 4.64 (sext, J = 6.4 Hz, 1H), 4.48 (br d, J = 4.9 Hz, 1H), 4.27 (td, J = 8.1, 3.3 Hz, 1H), 3.71 (dd, J = 13.4, 4.9 Hz, 1H), 3.29 (d, J = 13.0 Hz, 1H), 3.16−3.05 (m, 2H), 2.38−2.34 (m, 3H), 2.21 (s, 3H), 1.95−1.79 (m, 2H), 1.31 (d, J = 6.09 Hz, 3H); ^{13}C{^{1}H} NMR (100 MHz, D_2O): δ 172.2, 156.5, 130.1, 128.6, 117.0, 85.0, 76.9, 74.3, 71.9, 69.5, 61.9, 50.8, 34.1, 30.4, 20.1, 18.7 (18.7), 14.0 (13.6). HRMS (ESI$^+$) calcd m/z for $C_{19}H_{26}NO_4$ [M + H]$^+$ 332.1856; found, 332.1862.

*(2R,3S,4S)-4-Hydroxy-2-(4-propyloxybenzyl)pyrrolidin-3-yl Acetate Hydrochloride (**26**).* Employing the protocol used for the preparation of ether **20**, *N*-Boc-desmethylanisomycin (**13**, 25.0 mg, 0.0711 mmol, 100 mol %) in dry DMF (0.6 mL, 119 mM) was treated with Cs_2CO_3 (25.5 mg, 0.0786 mmol, 110 mol %) and propyl-4-methylbenzenesulfonate (19.8 mg, 0.0925 mmol, 130 mol %). After the mixture was heated at 66 °C for 3 h, TLC indicated complete reaction. After aqueous workup, the *N*-Boc-*O*-propyl ether [R_f = 0.55, 50% EtOAc in hexanes] was purified by flash chromatography (on a 30 cm × 1.5 cm fritted-disc column containing 15.4 g of silica gel) eluting with a gradient of 10−40% EtOAc in hexanes. Evaporation of the collected fractions under reduced pressure (bath temperature 40 °C) afforded a viscous colorless oil (18.5 mg, 66% yield): ^{1}H NMR (400 MHz, $CDCl_3$): δ 7.05 (d, J = 7.8 Hz, 2H), 6.79 (d, J = 8.6 Hz, 2H), 4.88 (t, J = 6.4 Hz, 1H), 4.44−4.35 (m, 1H), 4.00 (m, 1H), 3.87 (t, J = 6.6 Hz, 1H), 3.46 (m, 1H), 3.33 (m, 1H), 3.04−2.80 (m, 2H), 2.63 (m, 1H), 2.08 (s, 3H), 1.78 (sext, J = 7.31 Hz, 2H), 1.46 (s, 9H), 1.02 (t, J = 7.3 Hz, 3H).

The residue was dissolved in dry DCM (5.49 mL, 8.56 mM) and treated with HCl gas bubbles for 3 h, when TLC showed disappearance of the starting material and appearance of a ninhydrin and $KMnO_4$ active baseline spot (50% EtOAc in hexanes). The volatiles were evaporated. The residue was precipitated with diethyl ether (2 × 5 mL) and centrifuged to provide the desired *O*-propyl ether hydrochloride **26** as a white solid (13.5 mg, 87%): LC−MS analysis (λ = 214 nm), >99% purity [RT 4.30 min, 10−90% MeOH (0.1% FA) in H_2O (0.1% FA), and RT 5.76 min, 10−90% MeCN (0.1% FA) in H_2O (0.1% FA), over 14 min, respectively]. ^{1}H NMR (400 MHz, D_2O): δ 7.26 (d, J = 8.8 Hz, 2H), 7.01 (d, J = 8.8 Hz, 2H), 5.09 (d, J = 3.3 Hz, 1H), 4.47 (dt, J = 4.9, 1.2 Hz, 1H), 4.25 (td, J = 4.9, 1.4 Hz, 1H), 4.03 (t, J = 6.6 Hz, 2H), 3.70 (dd, J = 13.4, 5.1 Hz, 1H), 3.27 (d, J = 13.4 Hz, 1H), 3.15−3.03 (m, 2H), 2.21 (s, 3H), 1.77 (sext, 2H), 0.99 (t, J = 7.2 Hz, 3H); ^{13}C{^{1}H} NMR (100 MHz, D_2O): δ 172.2, 157.4, 130.0, 128.3, 115.3, 77.0, 72.1, 70.4, 61.9, 50.8, 30.5, 21.8, 20.1, 9.6. HRMS (ESI$^+$) calcd m/z for $C_{16}H_{24}NO_4$ [M + H]$^+$ 294.1699; found, 294.1697.

*(2R,3S,4S)-4-Hydroxy-2-(4-(pentyloxy)benzyl)pyrrolidin-3-yl Acetate Hydrochloride (**27**).* Employing the protocol used for the preparation of ether **20**, *N*-Boc-desmethylanisomycin (**13**, 25.0 mg, 0.0711 mmol, 100 mol %) in dry DMF (0.6 mL, 119 mM) was treated with Cs_2CO_3 (25.5 mg, 0.0783 mmol, 110 mol %) and pentyl-4-methylbenzenesulfonate (19.8 mg, 0.0925 mmol, 130 mol %). After the sample was heated at 77 °C for 90 min, TLC indicated complete reaction. After aqueous workup, the *N*-Boc-*O*-pentyl ether [R_f = 0.59, 50% EtOAc in hexanes] was purified by flash chromatography (on a 30 cm × 1.5 cm fritted-disc column containing 15.7 g of silica gel) eluting with a gradient of 10−35% of EtOAc in hexanes. Evaporation of the collected fractions under reduced pressure (bath temperature 40 °C) afforded a viscous colorless oil (13.2 mg, 44% yield): ^{1}H NMR (400 MHz, $CDCl_3$): δ 7.05 (d, J = 8.0 Hz, 2H), 6.80 (d, J = 8.4 Hz, 2H), 4.88 (t, J = 6.1 Hz, 1H), 4.40−4.36 (m, 1H), 4.00 (m, 1H), 3.91 (t, J = 6.5 Hz, 2H), 3.47 (m, 1H), 3.33 (m, 1H), 3.04−2.65 (m, 2H), 2.65 (m, 1H), 2.08 (s, 3H), 1.80−1.73 (m, 2H), 1.46 (s, 9H), 1.43−1.35 (m, 4H), 0.93 (t, J = 6.9 Hz, 3H).

After treatment of the residue in dry DCM (3.70 mL, 8.56 mM) with HCl gas bubbles for 1 h, TLC showed the disappearance of the starting material and the appearance of a ninhydrin and $KMnO_4$ active baseline spot (50% EtOAc in hexanes). The volatiles were evaporated. The residue was precipitated with diethyl ether (2 × 5 mL) and centrifuged to provide the desired *O*-pentyl ether hydrochloride **27** as a white solid (7.31 mg, 65%): LC−MS analysis (λ = 214 nm), >99% purity [RT 4.30 min, 10−90% MeOH (0.1% FA) in H_2O (0.1% FA), and RT 6.27 min, 10−90% MeCN (0.1% FA) in H_2O (0.1% FA), over 14 min, respectively]. ^{1}H NMR (400 MHz, D_2O): δ 7.25 (d, J = 8.2 Hz, 2H), 6.98 (d, J = 8.2 Hz, 2H), 5.08 (d, J = 2.9 Hz, 1H), 4.48 (d, J = 4.7 Hz, 1H), 4.25 (td, J = 8.3, 3.5 Hz, 1H), 4.05 (t, J = 6.6 Hz, 2H), 3.70 (dd, J = 13.7, 4.9 Hz, 1H), 3.29 (d, J = 13.3 Hz, 1H), 3.15−3.03 (m, 2H), 2.20 (s, 3H), 1.75 (quint, 2H), 1.44−1.29 (m, 4H), 0.88 (t, J = 7.0 Hz, 3H); ^{13}C{^{1}H} NMR (100 MHz, D_2O): δ 172.2, 157.4, 130.0, 128.2, 115.3, 76.8, 72.0, 68.8, 61.9, 50.8, 30.4, 28.0, 27.4, 21.8, 20.1, 13.3. HRMS (ESI$^+$) calcd m/z for $C_{18}H_{28}NO_4$ [M + H]$^+$ 322.2013; found, 322.2010.

*(2R,3S,4S)-4-Hydroxy-2-(4-(octyloxy)benzyl)pyrrolidin-3-yl Acetate Hydrochloride (**28**).* Employing the protocol used for the preparation of ether **20**, *N*-Boc-desmethylanisomycin (**13**, 18.0 mg, 0.0512 mmol, 100 mol %) in dry DMF (2.74 mL, 18.7 mM) was treated with Cs_2CO_3 (2.74 mL, 18.7 mM) and octyl iodide (14.8 mg, 0.0615 mmol, 130 mol %). After heating at 65 °C for 2 h, TLC indicated complete reaction. After aqueous workup, the *N*-Boc-*O*-octyl ether [R_f = 0.63, 50% EtOAc in hexanes] was purified by flash chromatography (on a 30 cm × 1.5 cm fritted-disc column containing 15.6 g of silica gel), eluting with a gradient of 10−35% EtOAc in hexanes. Evaporation of the collected fractions under reduced pressure (bath temperature 40 °C) afforded a viscous colorless oil (11.9 mg, 50% yield): ^{1}H NMR (400 MHz, CD_3OD): δ 7.07 (br d, 2H), 6.80 (d, J = 8.6 Hz, 2H), 4.80 (t, J = 5.6 Hz, 1H), 4.29 (ddd, J = 9.3, 6.0, 4.6 Hz, 1H), 4.05 (m, 1H), 3.92 (t, J = 6.4 Hz, 2H), 3.47−3.43 (m, 1H), 3.32−3.28 (m, 2H), 3.15 (br d, J = 13.1 Hz, 1H), 2.96 (br d, J = 11.0 Hz, 1H), 2.77−2.73 (m, 1H), 2.05 (s, 3H), 1.77−1.70 (m, 2H), 1.48−1.45 (m, 9H), 1.34−1.28 (m, 9H), 0.92−0.88 (m, 3H).

The residue was dissolved in dry DCM (3.00 mL, 8.56 mM) and treated with HCl gas bubbles. After 1 h, TLC showed the disappearance of the starting material and appearance of a ninhydrin and $KMnO_4$ active baseline spot (50% EtOAc in hexanes). The volatiles were evaporated. The residue was precipitated with diethyl ether (2 × 5 mL)

https://doi.org/10.1021/acs.jmedchem.5c01291
J. Med. Chem. 2025, 68, 20264−20282

and centrifuged to provide the desired *O*-octyl ether hydrochloride **28** as white solid (8.01 mg, 78%): LC−MS analysis (λ = 214 nm), >99% purity [RT 9.28 min, 10−90% MeOH (0.1% FA) in H_2O (0.1% FA), and RT 6.96 min, 10−90% MeCN (0.1% FA) in H_2O (0.1% FA), over 14 min, respectively]. ^{1}H NMR (400 MHz, CD_3OD): δ 7.21 (d, J = 8.8 Hz, 2H), 6.90 (d, J = 8.6 Hz, 2H), 5.07 (d, J = 3.2 Hz, 1H), 4.35 (br d, J = 4.7 Hz, 1H), 4.18 (dd, J = 6.7, 3.4 Hz, 1H), 4.15 (dd, J = 5.7, 2.4 Hz, 1H), 3.95 (t, J = 6.2 Hz, 2H), 3.58 (dd, J = 12.7, 4.4 Hz, 1H), 3.29 (d, J = 13.6 Hz, 1H), 3.08 (dd, J = 14.6, 7.1 Hz, 1H), 2.94 (dd, J = 14.3, 8.9 Hz, 1H), 2.18 (s, 3H), 1.79−1.72 (m, 2H), 1.50−1.43 (m, 2H), 1.38−1.29 (m, 8H) 0.90 (t, J = 7.0 Hz, 3H); ^{13}C{^{1}H} NMR (100 MHz, CD_3OD): δ 170.8, 160.1, 130.9, 128.8, 116.1, 78.3, 73.4, 69.1, 63.7, 52.6, 33.0, 32.2, 30.5, 30.4, 30.3, 27.1, 23.7, 20.6, 14.4. HRMS (ESI$^+$) calcd m/z for $C_{21}H_{34}NO_4$ [M + H]$^+$ 364.2475; found, 364.2482.

*(2R,3S,4S)-2-(4-(2-(2-Ethoxyethoxy)ethoxy)benzyl)-4-hydroxypyrrolidin-3-yl Acetate Hydrochloride (**29**).* Employing the protocol used for the preparation of ether **20**, *N*-Boc-desmethylanisomycin (**13**, 25.0 mg, 0.0711 mmol, 100 mol %) in dry DMF (0.6 mL, 119 mM) was treated with Cs_2CO_3 (25.5 mg, 0.0783 mmol, 110 mol %) and 2-(2-ethoxyethoxy)ethyl-4-methylbenzenesulfonate (26.7 mg, 0.0925 mmol, 130 mol %). After the mixture was heated at 70 °C for 90 min, TLC indicated complete reaction. After aqueous workup, the *N*-Boc-*O*-2-(2-ethoxyethoxy)ethyl ether [R_f = 0.47, 80% EtOAc in hexanes] was purified by flash chromatography (on a 30 cm × 1.5 cm fritted-disc column containing 15.6 g of silica gel) eluting with a gradient of 10−35% EtOAc in hexanes. Evaporation of the collected fractions under reduced pressure (bath temperature 40 °C) afforded a viscous colorless oil (25 mg, 75% yield): ^{1}H NMR (400 MHz, $CDCl_3$): δ 7.05 (d, J = 8.2 Hz, 2H), 6.81 (d, J = 8.5 Hz, 2H), 4.87 (t, J = 6.3 Hz, 1H), 4.39−4.35 (m, 1H), 4.09 (t, J = 4.5 Hz, 2H), 3.98 (m, 1H), 3.84 (t, J = 5.1 Hz, 2H), 3.72−3.69 (m, 2H), 3.62−3.59 (m, 2H), 3.53 (q, J = 7.0 Hz, 2H), 3.45 (m, 1H), 3.31 (m, 1H), 3.04−2.80 (m, 2H), 2.66 (m, 1H), 2.08 (s, 3H), 1.46 (s, 9H), 1.21 (t, J = 6.9 Hz, 3H).

After treating the residue in dry DCM (3.70 mL, 8.56 mM) with HCl gas bubbles for 1 h, TLC showed the disappearance of the starting material and the appearance of a ninhydrin and $KMnO_4$ active baseline spot (80% EtOAc in hexanes). The volatiles were evaporated. The residue was precipitated with diethyl ether (2 × 5 mL) and centrifuged to provide the desired *O*-2-(2-ethoxyethoxy)ethyl ether hydrochloride **29** as a sticky light yellow oil (19.5 mg, 90%): LC−MS analysis (λ = 214 nm), >99% purity [RT 3.79 min, 10−90% MeOH (0.1% FA) in H_2O (0.1% FA), and RT 5.36 min, 10−90% MeCN (0.1% FA) in H_2O (0.1% FA), over 14 min, respectively]. ^{1}H NMR (400 MHz, D_2O): δ 7.28 (d, J = 8.9 Hz, 2H), 7.02 (d, J = 8.6 Hz, 2H), 5.11 (d, J = 3.2 Hz, 1H), 4.49 (br d, J = 4.7 Hz, 1H), 4.29−4.25 (m, 1H), 4.23−4.21 (m, 2H), 3.89−3.87 (m, 2H), 3.75−3.71 (m, 3H), 3.69−3.65 (m, 3H), 3.58 (q, J = 7.2 Hz, 2H), 3.28 (d, J = 13.3 Hz, 1H) 3.16−3.04 (m, 2H), 2.21 (s, 3H), 1.18 (t, J = 7.1 Hz, 3H); ^{13}C{^{1}H} NMR (100 MHz, D_2O): δ 172.2, 157.2, 130.0, 128.5, 115.3, 76.9, 72.0, 69.7, 69.0, 68.9, 67.2, 66.6, 61.9, 50.8, 30.4, 20.1, 14.0. HRMS (ESI$^+$) calcd m/z for $C_{19}H_{30}NO_6$ [M + H]$^+$ 368.2068; found, 368.2050.

Pent-4-yn-1-yl-4-Methylbenzenesulfonate. In a flame-dried 100 mL round-bottom flask fitted with 24 mm rubber septum and 15 mm × 7.5 mm cylindrical PTFE coated magnetic stir bar under an inert N_2 atmosphere, a solution of pent-4-yn-1-ol (841 mg, 10 mmol, 100 mol %), triethylamine (1.32 g, 13 mmol, 130 mol %), and DMAP (122 mg, 1 mmol, 10 mol %) in dry DCM (56 mL, 179 mM) was cooled to 0 °C and treated portion-wise over 30 min with five portions (420 mg per portion) of *p*-toluene sulfonyl chloride (2.10 g, 11 mmol, 110 mol %). The reaction mixture was warmed to rt and stirred for 6 h, when TLC showed the disappearance of the alcohol spot and the appearance of a less polar spot. The reaction mixture was diluted with DCM (30 mL) and washed with water (20 mL) and brine (20 mL). The organic layer was dried over $NaSO_4$, filtered, and concentrated under reduced pressure. The reduced volume was passed through a pad of silica to remove residual 4-dimethylaminopyridinium chloride. The silica pad was eluted with ethyl acetate to obtain pent-4-yn-1-yl tosylate (1.86 g, 78% yield) as a light orange oil: R_f = 0.60 (20% EtOAc in hexanes). ^{1}H NMR (400 MHz, $CDCl_3$): δ 7.78 (d, J = 8.5 Hz, 2H), 7.34 (d, J = 8.1 Hz, 2H), 4.13 (t, J = 6.1 Hz, 2H), 2.44 (s, 3H), 2.25 (td, J = 6.9, 2.6 Hz, 2H), 1.88−1.82 (m, 3H); ^{13}C{^{1}H} NMR (100 MHz, $CDCl_3$): δ 145.0, 133.1, 130.0, 128.1, 82.2, 69.6, 68.9, 27.9, 21.8, 14.8. HRMS (ESI$^+$) calcd m/z for $C_{12}H_{15}O_3S$ [M + H]$^+$ 239.0736; found, 239.0731.

Hex-5-yn-1-yl 4-Methylbenzenesulfonate. Employing the protocol used for the preparation of pent-4-yn-1-yl-4-methylbenzenesulfonate, hex-5-yn-1-ol (300 mg, 3.06 mmol, 100 mol %), triethylamine (402 mg, 3.97 mmol, 130 mol %), and DMAP (37.3 mg, 0.31 mmol, 10 mol %) in dry DCM (17 mL, 180 mM) were treated with *p*-toluene sulfonyl chloride (641 mg, 3.36 mmol, 110 mol %). After 6 h, TLC indicated the disappearance of the alcohol spot and the appearance of a less polar spot. Following aqueous workup and filtration through a pad of silica, hex-5-yn-1-yl tosylate (661 mg, 86% yield) was obtained as a pale-yellow oil: R_f = 0.21, (10% EtOAc in hexanes). ^{1}H NMR (400 MHz, $CDCl_3$): δ 7.76 (d, J = 8.5 Hz, 2H), 7.33 (d, J = 7.9 Hz, 2H), 4.03 (t, J = 6.4 Hz, 2H), 2.43 (s, 3H), 2.14 (td, J = 6.9, 2.5 Hz, 2H), 1.90 (t, J = 2.6 Hz, 1H), 1.79−1.72 (m, 2H), 1.57−1.49 (m, 2H); ^{13}C{^{1}H} NMR (100 MHz, $CDCl_3$): δ 144.9, 133.2, 130.0, 128.0, 83.5, 70.0, 69.1, 27.8, 24.3, 21.7, 17.8. HRMS (ESI$^+$) calcd m/z for $C_{13}H_{17}O_3S$ [M + H]$^+$ 253.0893; found, 253.0887.

Hept-6-yn-1-yl 4-Methylbenzenesulfonate. Employing the protocol used for the preparation of pent-4-yn-1-yl-4-methylbenzenesulfonate, hept-6-yn-1-ol (1.0 g, 8.92 mmol, 100 mol %), triethylamine (1.17 g, 11.6 mmol, 130 mol %), and DMAP (109 mg, 0.89 mmol, 10 mol %) in dry DCM (45 mL, 175 mM) were treated with *p*-toluene sulfonyl chloride (1.87 g, 9.81 mmol, 110 mol %). After 3 h, TLC indicated the disappearance of the alcohol spot and the appearance of a less polar spot. Following aqueous workup and filtration through a pad of silica, hept-6-yn-1-yl tosylate (1.99 g, 84% yield) was obtained as a colorless oil: R_f = 0.46, (25% EtOAc in hexanes). ^{1}H NMR (400 MHz, $CDCl_3$): δ 7.78 (d, J = 8.3 Hz, 2H), 7.34 (d, J = 7.9 Hz, 2H), 4.02 (t, J = 6.5 Hz, 2H), 2.44 (s, 3H), 2.14 (td, J = 6.8, 2.9 Hz, 2H), 1.92 (t, J = 2.8 Hz, 1H), 1.66 (quint, 2H), 1.51−1.40 (m, 4H); ^{13}C{^{1}H} NMR (100 MHz, $CDCl_3$): δ 144.9, 133.3, 130.0, 128.0, 84.1, 70.5, 68.7, 28.5, 27.8, 24.6, 21.8, 18.3. HRMS (ESI$^+$) calcd m/z for $C_{14}H_{18}O_3KS$ [M + K]$^+$ 305.0608; found, 305.0603.

Oct-7-yn-1-yl 4-Methylbenzenesulfonate. Employing the protocol used for the preparation of pent-4-yn-1-yl-4-methylbenzenesulfonate, oct-7-yn-1-ol (300 mg, 2.38 mmol, 100 mol %), triethylamine (313 mg, 3.09 mmol, 130 mol %), and DMAP (29 mg, 0.24 mmol, 10 mol %) in dry DCM (13 mL, 183 mM) were treated with *p*-toluene sulfonyl chloride (499 mg, 2.61 mmol, 110 mol %). After 6 h, TLC indicated the disappearance of the alcohol spot and the appearance of a less polar spot. Following aqueous workup and filtration through a pad of silica, oct-7-yn-1-yl tosylate (567 mg, 84% yield) was obtained as a colorless oil: R_f = 0.94 (20% EtOAc in hexanes). ^{1}H NMR (400 MHz, $CDCl_3$): δ 7.75 (d, J = 8.5 Hz, 2H), 7.32 (d, J = 8.5 Hz, 2H), 3.99 (t, J = 6.5 Hz, 2H), 2.42 (s, 3H), 2.14 (td, J = 6.8, 2.9 Hz, 2H), 1.92 (t, J = 2.8 Hz, 1H), 1.66 ; found, (quint, 2H), 1.47−1.40 (m, 2H), 1.33−1.28 (m, 4H); ^{13}C{^{1}H} NMR (100 MHz, $CDCl_3$): δ 144.8, 133.2, 129.9, 127.9, 84.4, 70.6, 68.4, 28.7, 28.2, 28.0, 24.9, 21.7, 18.3. HRMS (ESI$^+$) calcd m/z for $C_{15}H_{24}NO_3S$ [M + NH_4]$^+$ 298.1471; found, 298.1469.

Hex-5-yn-2-yl 4-Methylbenzenesulfonate. Employing the protocol used for the preparation of pent-4-yn-1-yl-4-methylbenzenesulfonate, hex-5-yn-2-yl-ol (78.3 mg, 0.78 mmol, 100 mol %), triethylamine (105 mg, 1.04 mmol, 130 mol %), and DMAP (0.75 mg, 0.08 mmol, 10 mol %) in dry DCM (4.5 mL, 177 mM) were treated with *p*-toluene sulfonyl chloride (167 mg, 0.878 mmol, 110 mol %). After 6 h, TLC indicated the disappearance of the alcohol spot and the appearance of a less polar spot. Following aqueous workup and filtration through a pad of silica gel, hex-5-yn-2-yl tosylate (107 mg, 53% yield) was obtained as a brown oil: R_f = 0.43, (20% EtOAc in hexanes). ^{1}H NMR (400 MHz, $CDCl_3$): δ 7.79 (d, J = 8.3 Hz, 2H), 7.32 (d, J = 8.0 Hz, 2H), 4.76−4.69 (m, 1H), 2.44 (s, 3H) (2.40 (s, 0.2H)), 2.22−2.02 (m, 2H), 1.87 (t, J = 2.7 Hz, 1H), 1.86−1.78 (m, 1H), 1.75−1.66 (m, 1H), 1.30 (d, J = 6.3 Hz, 3H) (1.38 (d, J = 6.4 Hz, 0.3H)); ^{13}C{^{1}H} NMR (100 MHz, $CDCl_3$): δ 144.7, 134.4, 129.9 (129.7), 127.8 (128.0), 82.7, 78.9, 69.2, 35.4, 21.7(22.1), 20.9, 14.6(14.3). HRMS (ESI$^+$) calcd m/z for $C_{13}H_{17}O_3S$ [M + H]$^+$ 253.0889; found, 253.0893.

Propyl 4-Methylbenzenesulfonate. Employing the protocol used for the preparation of pent-4-yn-1-yl-4-methylbenzenesulfonate, 1-

https://doi.org/10.1021/acs.jmedchem.5c01291
J. Med. Chem. 2025, 68, 20264−20282

propanol (1.0 g, 16.6 mmol, 100 mol %), triethylamine (2.19 g, 21.6 mmol, 130 mol %), and DMAP (203 mg, 1.66 mmol, 10 mol %) in dry DCM (90 mL, 163 mM) were treated with *p*-toluene sulfonyl chloride (3.5 g, 18.3 mmol, 110 mol %). After 3 h, TLC indicated the disappearance of the alcohol spot and the appearance of a less polar spot. Following aqueous workup and filtration through a pad of silica gel, propyl tosylate (quantitative yield) was obtained as a colorless oil: R_f = 0.58 (10% EtOAc in hexanes). ^{1}H NMR (400 MHz, $CDCl_3$): δ 7.77 (d, J = 8.4 Hz, 2H), 7.33 (d, J = 8.1 Hz, 2H), 3.97 (t, J = 6.5 Hz, 2H), 2.43 (s, 3H), 2.14 (td, J = 6.8, 2.9 Hz, 2H), 1.92 (t, J = 2.8 Hz, 1H), 1.65 (quint, 2H), 0.88 (t, J = 7.5 Hz, 4H); ^{13}C{^{1}H} NMR (100 MHz, $CDCl_3$): δ 144.8, 133.3, 129.9, 127.9, 72.3, 22.4, 21.7, 10.0. HRMS (ESI$^+$) calcd m/z for $C_{10}H_{15}O_3S$ $[M + H]^+$ 215.0736; found, 215.0731.

Pentyl 4-Methylbenzenesulfonate. Employing the protocol used for the preparation of pent-4-yn-1-yl-4-methylbenzenesulfonate, 1-pentanol (1.0 g, 11.3 mmol, 100 mol %), triethylamine (1.5 g, 14.7 mmol, 130 mol %), and DMAP (139 mg, 1.13 mmol, 10 mol %) in dry DCM (62 mL, 163 mM) were treated with *p*-toluene sulfonyl chloride (2.4 g, 12.5 mmol, 110 mol %). After 3 h, TLC indicated the disappearance of the alcohol spot and the appearance of a less polar spot. Following aqueous workup and filtration through a pad of silica gel, pentyl tosylate (quantitative yield) was obtained as a peach orange oil: R_f = 0.92, (50% EtOAc in hexanes). ^{1}H NMR (400 MHz, $CDCl_3$): δ 7.78 (d, J = 8.3 Hz, 2H), 7.34 (d, J = 8.0 Hz, 2H), 4.01 (t, J = 6.7 Hz, 2H), 2.44 (s, 3H), 1.66−1.59 (m, 2H), 1.27−1.24 (m, 4H) 0.84 (t, J = 7.0 Hz, 3H); ^{13}C{^{1}H} NMR (100 MHz, $CDCl_3$): δ 144.8, 133.4, 129.9, 128.0, 70.8, 28.6, 27.6, 22.2, 21.8, 13.9. HRMS (ESI$^+$) calcd m/z for $C_{12}H_{19}O_3S$ $[M + H]^+$ 243.1049; found, 243.1045.

2-(2-Ethoxyethoxy)ethyl 4-Methylbenzenesulfonate. Employing the protocol used for the preparation of pent-4-yn-1-yl-4-methylbenzenesulfonate, 2-(2-ethoxyethoxy)ethan-1-ol (500 mg, 3.73 mmol, 100 mol %), triethylamine (490 mg, 4.84 mmol, 130 mol %), and DMAP (45.5 mg, 0.37 mmol, 10 mol %) in dry DCM (20 mL, 163 mM) were treated with *p*-toluene sulfonyl chloride (781 mg, 4.10 mmol, 110 mol %). After 3 h, TLC indicated the disappearance of the alcohol spot and the appearance of a less polar spot. Following aqueous workup and filtration through a pad of silica, the 2-(2-ethoxyethoxy)ethyl tosylate (698 mg, 65% yield) was obtained as a colorless oil: R_f = 0.32, (30% EtOAc in hexanes). ^{1}H NMR (400 MHz, $CDCl_3$): δ 7.78 (d, J = 8.3 Hz, 2H), 7.32 (d, J = 7.9 Hz, 2H), 4.16−414 (m, 2H), 3.69−3.67 (m, 2H), 3.58−3.55 (m, 2H), 3.51−3.50 (m, 2H), 3.49−3.48 (m, 1H), 3.46 (d, 1H), 2.43 (s, 3H), 1.17 (t, J = 7.0 Hz, 3H); ^{13}C{^{1}H} NMR (100 MHz, $CDCl_3$): δ 144.9, 133.1, 129.9, 128.1, 70.9, 69.8, 69.4, 68.8, 66.8, 21.7, 15.2. HRMS (ESI$^+$) calcd m/z for $C_{13}H_{21}O_5S$ $[M + H]^+$ 289.1104; found, 289.1099.

■ ASSOCIATED CONTENT

Data Availability Statement

The cryo-EM density map of the *L. major* 80S ribosome bound to **20** has been deposited in the Electron Microscopy Data Bank (EMDB) under accession number EMD-52247. Atomic coordinates and structure factors have been deposited in the Protein Data Bank (PDB) under accession code 9HL9.

Supporting Information

The Supporting Information is available free of charge at https://pubs.acs.org/doi/10.1021/acs.jmedchem.5c01291.

GO name, protein count, treatment, strength, and FDR (XLSX)

SMILES data (CSV)

Conserved binding pocket, summary of proteins, NMR spectrum, HRMS spectrum, and LC-MS reports (PDF)

Well-defined density observed for *O*-propargyl ether **20** near the peptidyl transferase center (MP4)

■ AUTHOR INFORMATION

Corresponding Authors

Christopher Fernandez-Prada − *Department of Pathology and Microbiology, Faculty of Veterinary Medicine, Université de Montréal, Saint-Hyacinthe, Quebec J2S 2M2, Canada; The Research Group on Infectious Diseases in Production Animals (GREMIP), Faculty of Veterinary Medicine, Université de Montréal, Saint-Hyacinthe, Quebec J2S 2M2, Canada;* orcid.org/0000-0003-4834-4956; Email: christopher.fernandez.prada@umontreal.ca

Martin Olivier − *Departments of Medicine, and of Microbiology and Immunology, Faculty of Medicine, McGill University, Montréal, Quebec H3A 2B4, Canada; The Research Institute of the McGill University Health Centre, Montréal, Quebec H4A 3J1, Canada*; Email: martin.olivier@mcgill.ca

Ada Yonath − *Department of Chemical and Structural Biology, Weizmann Institute of Science, Rehovot 7610001, Israel*; Email: Ada.Yonath@weizmann.ac.il

William D. Lubell − *Department of Chemistry, Université de Montréal, Montréal, Quebec H2 V 0B3, Canada;* orcid.org/0000-0002-3080-2712; Email: william.lubell@umontreal.ca

Authors

Kajumee Bora Bhowal − *Department of Chemistry, Université de Montréal, Montréal, Quebec H2 V 0B3, Canada;* orcid.org/0009-0001-6154-1746

Anh Minh Thao Nguyen − *Department of Chemistry, Université de Montréal, Montréal, Quebec H2 V 0B3, Canada*

Ana Victoria Ibarra-Meneses − *Department of Pathology and Microbiology, Faculty of Veterinary Medicine, Université de Montréal, Saint-Hyacinthe, Quebec J2S 2M2, Canada; The Research Group on Infectious Diseases in Production Animals (GREMIP), Faculty of Veterinary Medicine, Université de Montréal, Saint-Hyacinthe, Quebec J2S 2M2, Canada*

Andressa Brito Lira − *Departments of Medicine, and of Microbiology and Immunology, Faculty of Medicine, McGill University, Montréal, Quebec H3A 2B4, Canada; The Research Institute of the McGill University Health Centre, Montréal, Quebec H4A 3J1, Canada*

K. Shanmugha Rajan − *Department of Chemical and Structural Biology, Weizmann Institute of Science, Rehovot 7610001, Israel;* orcid.org/0000-0003-4826-9802

Jesus D. Castaño − *Département de Biomédecine Vétérinaire, Faculté de Médecine Vétérinaire, Université de Montréal, Saint-Hyacinthe, Quebec J2S 2M2, Canada;* orcid.org/0000-0003-1947-2203

Francis Beaudry − *Département de Biomédecine Vétérinaire, Faculté de Médecine Vétérinaire, Université de Montréal, Saint-Hyacinthe, Quebec J2S 2M2, Canada*

Anat Bashan − *Department of Chemical and Structural Biology, Weizmann Institute of Science, Rehovot 7610001, Israel*

Complete contact information is available at: https://pubs.acs.org/10.1021/acs.jmedchem.5c01291

Author Contributions

KBB performed the chemical synthesis and contributed to the writing of the original draft of the manuscript. AMTN contributed preliminary peptide conjugates. AVIM conducted the experimentation on *Leishmania* strains. AVIM, JDC, and FB conducted the thermal proteomic profiling and gene ontology analyses. ABL performed the experiments on *Trypanosoma* and conducted cytotoxicity studies. KSR and AB developed the cryo-

https://doi.org/10.1021/acs.jmedchem.5c01291
J. Med. Chem. 2025, 68, 20264−20282

EM studies. All authors provided the corresponding experimental procedures. WDL conceptualized the study. WDL, CFP, MO, AB, and AY obtained project funding and directed the project. WDL, CFP, MO, AB, and AY critically reviewed and revised the manuscript. All authors have read and approved the final version of the manuscript.

Notes

The authors declare no competing financial interest.

■ ACKNOWLEDGMENTS

We thank Prof. David Langlais for kindly providing the BMDM cells used in this study. We are grateful for funding from the Natural Sciences and Engineering Research Council of Canada (NSERC, Discovery Research Project RGPIN-2019-04079), the Canadian Institutes of Health Research (CIHR Project PJT-18054), and the Fonds de Recherche du Québec - Nature et Technologie for support of the Centre in Green Chemistry and Catalysis (CGCC, FRQNT-2020-RS4-265155-CCVC). Operation of the NMR spectrometers at the Regional Centre for Magnetic Resonance in the Department of Chemistry at the Université de Montréal was made possible through funding from the Canada Foundation for Innovation and the Institute Courtois. K.S.R. is supported by the Senior-Postdoctoral Fellowship from the Weizmann Institute of Science. A.Y. holds the Martin S. and Helen Kimmel Professorial Chair at the Weizmann Institute of Science. Assistance is acknowledged from members of the Université de Montréal facilities: Dr. P. Aguiar (NMR spectroscopy) and Dr. A. Fürtös (mass spectrometry).

■ ABBREVIATIONS

ΔT, change in melting temperature; A-site, acceptor site; AmB, amphotericin B; ANM, anisomycin; API, atmospheric pressure ionization; BHT, butylated hydroxytoluene; BMDM, bone marrow derived cells; Bt, benzotriazole; CC_{50}, 50% Cytotoxicity Concentration; CD, chagas disease; DMF, dimethylformamide; *E. coli*, *Escherichia coli*; EM, electron microscopy; E, site exit site; FA, formic acid; FSC, Fourier shell correlation; GO, gene ontology; HAT, Human African Trypanosomiasis; *H. marismortui*, *Haloarcula marismortui*; HSP70, heat shock protein 70; HSP83, heat shock protein 83; *L. Infantum*, *Leishmania Infantum*; *Li* AmB-res, *Leishmania Infantum* amphotericin B resistant; *Li* SB-res, *Leishmania Infantum* antimony-resistant; *Li* MF-res, *Leishmania Infantum* miltefosine-resistant; *Li*WT, *Leishmania Infantum* wild type; *Lm*F, *Leishmania major* Friedlin; LSU, large subunit; MF, Miltefosine; MSD, mass selective detector; MTT, 3-(4,5-dimethylthiazol-2-yl)-2,5-diphenyltetrazolium bromide; NTD, neglected tropical diseases; P-site, peptidyl site; PTC, peptidyl transferase center; PTFE, polytetrafluoroethylene; PTSA, *p*-toluene sulfonic acid; RNS, reactive nitrogen species; RT, retention time; S, Svedbergs unit; SB, antimony; SI, selectivity index; SPA, single-particle cryo-EM analysis; SSU, small subunit; *T. brucei*, *Trypanosoma brucei*; *T. cruzi*, *Trypanosoma cruzi*; TPP, thermal proteomic profiling

■ REFERENCES

(1) Casulli, A. New Global Targets for NTDs in the WHO Roadmap 2021−2030. *PLoS Neglected Trop. Dis.* **2021**, *15* (5), No. e0009373.
(2) *Leishmaniasis*. https://www.who.int/news-room/fact-sheets/detail/leishmaniasis (accessed on July 2025).
(3) *Trypanosomiasis, Human African (Sleeping Sickness)*. https://www.who.int/news-room/fact-sheets/detail/trypanosomiasis-human-african-(sleeping-sickness) (accessed on July 2025).
(4) *Chagas Disease (Also Known as American Trypanosomiasis)*. https://www.who.int/news-room/fact-sheets/detail/chagas-disease-(american-trypanosomiasis) (accessed on July 2025).
(5) Baker, R. E.; Mahmud, A. S.; Miller, I. F.; Rajeev, M.; Rasambainarivo, F.; Rice, B. L.; Takahashi, S.; Tatem, A. J.; Wagner, C. E.; Wang, L. F.; Wesolowski, A.; Metcalf, C. J. E. Infectious Disease in an Era of Global Change. *Nat. Rev. Microbiol.* **2022**, *20* (4), 193−205.
(6) Bamorovat, M.; Sharifi, I.; Khosravi, A.; et al. Global Dilemma and Needs Assessment Toward Achieving Sustainable Development Goals in Controlling Leishmaniasis. *J. Epidemiol. Global Health* **2024**, *14*, 22−34.
(7) Autheman, D.; Crosnier, C.; Clare, S.; Goulding, D. A.; Brandt, C.; Harcourt, K.; Tolley, C.; Galaway, F.; Khushu, M.; Ong, H.; Romero-Ramirez, A.; Duffy, C. W.; Jackson, A. P.; Wright, G. J. An Invariant Trypanosoma Vivax Vaccine Antigen Induces Protective Immunity. *Nature* **2021**, *595* (7865), 96−100.
(8) Ziegelbauer, K.; Overath, P. Organization of Two Invariant Surface Glycoproteins in the Surface Coat of Trypanosoma Brucei. *Infect. Immun.* **1993**, *61* (11), 4540−4545.
(9) Beaumier, C. M.; Gillespie, P. M.; Strych, U.; Hayward, T.; Hotez, P. J.; Bottazzi, M. E. Status of Vaccine Research and Development of Vaccines for Chagas Disease. *Vaccine* **2016**, *34* (26), 2996−3000.
(10) Quijano-Hernandez, I.; Dumonteil, E. Advances and Challenges toward a Vaccine against Chagas Disease. *Hum. Vaccines* **2011**, *7* (11), 1184−1191.
(11) Rodríguez-Morales, O.; Monteón-Padilla, V.; Carrillo-Sánchez, S. C.; Rios-Castro, M.; Martínez-Cruz, M.; Carabarin-Lima, A.; Arce-Fonseca, M. Experimental Vaccines against Chagas Disease: A Journey through History. *J. Immunol. Res.* **2015**, *2015*, 489758.
(12) Dujardin, J. C.; González-Pacanowska, D.; Croft, S. L.; Olesen, O. F.; Späth, G. F. Collaborative Actions in Anti-Trypanosomatid Chemotherapy with Partners from Disease Endemic Areas. *Trends Parasitol.* **2010**, *26* (8), 395−403.
(13) Filardy, A. A.; Guimarães-Pinto, K.; Nunes, M. P.; Zukeram, K.; Fliess, L.; Pereira, L.; Oliveira Nascimento, D.; Conde, L.; Morrot, A. Human Kinetoplastid Protozoan Infection: Where Are We Next? *Front. Immunol.* **2018**, *9*, 1493.
(14) Ponte-Sucre, A.; Gamarro, F.; Dujardin, J. C.; Barrett, M. P.; López-Vélez, R.; García-Hernández, R.; Pountain, A. W.; Mwenechanya, R.; Papadopoulou, B. Drug Resistance and Treatment Failure in Leishmaniasis: A 21st Century Challenge. *PLoS Neglected Trop. Dis.* **2017**, *11* (12), No. e0006052.
(15) Ponte-Sucre, A. An Overview of Trypanosoma Brucei Infections: An Intense Host−Parasite Interaction. *Front. Microbiol.* **2016**, *7*, 2126.
(16) Lidani, K. C. F.; Andrade, F. A.; Bavia, L.; Damasceno, F. S.; Beltrame, M. H.; Messias-Reason, I. J.; Sandri, T. L. Chagas Disease: From Discovery to a Worldwide Health Problem. *Front. Public Health* **2019**, *7*, 166.
(17) Bonney, K. M.; Engman, D. M. Chagas Heart Disease Pathogenesis: One Mechanism or Many? *Curr. Mol. Med.* **2008**, *8* (6), 510−518.
(18) Dickie, E. A.; Giordani, F.; Gould, M. K.; Mäser, P.; Burri, C.; Mottram, J. C.; Rao, S. P. S.; Barrett, M. P. New Drugs for Human African Trypanosomiasis: A Twenty First Century Success Story. *Trop. Med. Infect. Dis.* **2020**, *5* (1), 29.
(19) Temraz, M. G.; Elzahhar, P. A.; El-Din, A.; Bekhit, A.; Bekhit, A. A.; Labib, H. F.; Belal, A. S. F. Anti-Leishmanial Click Modifiable Thiosemicarbazones: Design, Synthesis, Biological Evaluation and in Silico Studies. *Eur. J. Med. Chem.* **2018**, *151*, 585−600.
(20) Pacheco, P. A. F.; Santos, M. M. M. Recent Progress in the Development of Indole-Based Compounds Active against Malaria, Trypanosomiasis and Leishmaniasis. *Molecules* **2022**, *27* (1), 319.
(21) Ciccone, V.; Diotallevi, A.; Gómez-Benmansour, M.; Maestrini, S.; Mantellini, F.; Mari, G.; Galluzzi, L.; Lucarini, S.; Favi, G. Easy One-Pot Synthesis of Multifunctionalized Indole−Pyrrole Hybrids as a New Class of Antileishmanial Agents. *RSC Adv.* **2024**, *14* (22), 15713−15720.

https://doi.org/10.1021/acs.jmedchem.5c01291
J. Med. Chem. 2025, 68, 20264−20282

(22) Bernhard, S.; Kaiser, M.; Burri, C.; Mäser, P. Fexinidazole for Human African Trypanosomiasis, the Fruit of a Successful Public-Private Partnership. *Diseases* **2022**, *10* (4), 90.
(23) Wyllie, S.; Foth, B. J.; Kelner, A.; Sokolova, A. Y.; Berriman, M.; Fairlamb, A. H. Nitroheterocyclic Drug Resistance Mechanisms in Trypanosoma Brucei. *J. Antimicrob. Chemother.* **2016**, *71* (3), 625−634.
(24) Kumeso, V. K. B.; Kalonji, W. M.; Rembry, S.; Mordt, O. V.; Tete, D. N.; Prêtre, A.; Delhomme, S.; Kyhi, M. I. W.; Camara, M.; Catusse, J.; Schneitter, S.; Nusbaumer, M.; Miaka, E. M.; Mbembo, H. M.; Mayawula, J. M.; Camara, M. L.; Massa, F. A.; Kaninda Badibabi, L.; Kasongo Bonama, A.; Lukula, P. K.; Kalonji, S. M.; Philemon, P. M.; Nganyonyi, R. M.; Mankiara, H. E.; Nguba, A. A. A.; Kobo Muanza, V.; Nasandhel, E. M.; Fifi, A.; Bambuwu, A. F. N.; Scherrer, B.; Strub-Wourgaft, N.; Tarral, A. Efficacy and Safety of Acoziborole in Patients with Human African Trypanosomiasis Caused by Trypanosoma Brucei Gambiense: A Multicentre, Open-Label, Single-Arm, Phase 2/3 Trial. *Lancet Infect. Dis.* **2023**, *23*, 463−470.
(25) Braillard, S.; Keenan, M.; Breese, K. J.; Heppell, J.; Abbott, M.; Islam, R.; Shackleford, D. M.; Katneni, K.; Crighton, E.; Chen, G.; Patil, R.; Lee, G.; White, K. L.; Carvalho, S.; Wall, R. J.; Chemi, G.; Zuccotto, F.; González, S.; Marco, M.; Deakyne, J.; Standing, D.; Brunori, G.; Lyon, J. J.; Castañeda-Casado, P.; Camino, I.; Martinez Martinez, M. S.; Zulfiqar, B.; Avery, V. M.; Feijens, P.-B.; Van Pelt, N.; Matheeussen, A.; Hendrickx, S.; Maes, L.; Caljon, G.; Yardley, V.; Wyllie, S.; Charman, S. A.; Chatelain, E. DNDI-6174 Is a Preclinical Candidate for Visceral Leishmaniasis That Targets the Cytochrome Bc1. *Sci. Transl. Med.* **2023**, *15* (726), 9902.
(26) Rimle, L.; Pliatsika, D.; Arnold, N.; Kurth, S.; Kaiser, M.; Mäser, P.; Kemmler, M.; Adams, M.; Riedl, R.; von Ballmoos, C. Dissecting Structural Requirements of Leucinostatin A Derivatives for Anti-protozoal Activity and Mammalian Toxicity. *J. Med. Chem.* **2025**, *68* (4), 4237−4258.
(27) Cavalli, A.; Bolognesi, M. L. Neglected Tropical Diseases: Multi-Target-Directed Ligands in the Search for Novel Lead Candidates against *Trypanosoma and Leishmania*. *J. Med. Chem.* **2009**, *52* (23), 7339−7359.
(28) Bustamante, J. M.; Craft, J. M.; Crowe, B. D.; Ketchie, S. A.; Tarleton, R. L. New, Combined, and Reduced Dosing Treatment Protocols Cure Trypanosoma Cruzi Infection in Mice. *J. Infect. Dis.* **2014**, *209* (1), 150−162.
(29) Schmid, C.; Kuemmerle, A.; Blum, J.; Ghabri, S.; Kande, V.; Mutombo, W.; Ilunga, M.; Lumpungu, I.; Mutanda, S.; Nganzobo, P.; Tete, D.; Mubwa, N.; Kisala, M.; Blesson, S.; Mordt, O. V. In-Hospital Safety in Field Conditions of Nifurtimox Eflornithine Combination Therapy (NECT) for T. b. Gambiense Sleeping Sickness. *PLoS Neglected Trop. Dis.* **2012**, *6* (11), No. e1920.
(30) Alonso-Vega, C.; Urbina, J. A.; Sanz, S.; Pinazo, M.-J.; Pinto, J. J.; Gonzalez, V. R.; Rojas, G.; Ortiz, L.; Garcia, W.; Lozano, D.; Soy, D.; Maldonado, R. A.; Nagarkatti, R.; Debrabant, A.; Schijman, A.; Thomas, M. C.; López, M. C.; Michael, K.; Ribeiro, I.; Gascon, J.; Torrico, F.; Almeida, I. C. New Chemotherapy Regimens and Biomarkers for Chagas Disease: The Rationale and Design of the TESEO Study, an Open-Label, Randomised, Prospective, Phase-2 Clinical Trial in the Plurinational State of Bolivia. *BMJ Open* **2021**, *11* (12), No. e052897.
(31) Morphy, R.; Rankovic, Z. Designed Multiple Ligands. An Emerging Drug Discovery Paradigm. *J. Med. Chem.* **2005**, *48* (21), 6523−6543.
(32) Gandini, A.; Prati, F.; Uliassi, E.; Bolognesi, M. L. Drug Discovery Strategies for the Generation of Multitarget Ligands Against Neglected Tropical Diseases. In *Drug Selectivity: An Evolving Concept in Medicinal Chemistry*; Handler, N., Buschmann, H., Eds.; Wiley VCH: Weinheim, Germany, 2017; pp 135−159.
(33) Belluti, F.; Uliassi, E.; Veronesi, G.; Bergamini, C.; Kaiser, M.; Brun, R.; Viola, A.; Fato, R.; Michels, P. A. M.; Krauth-Siegel, R. L.; Cavalli, A.; Bolognesi, M. L. Toward the Development of Dual-Targeted Glyceraldehyde-3-Phosphate Dehydrogenase/Trypanothione Reductase Inhibitors against Trypanosoma Brucei and Trypanosoma Cruzi. *ChemMedChem* **2014**, *9* (2), 371−382.
(34) Uliassi, E.; Fiorani, G.; Krauth-Siegel, R. L.; Bergamini, C.; Fato, R.; Bianchini, G.; Carlos Menéndez, J.; Molina, M. T.; López-Montero, E.; Falchi, F.; Cavalli, A.; Gul, S.; Kuzikov, M.; Ellinger, B.; Witt, G.; Moraes, C. B.; Freitas-Junior, L. H.; Borsari, C.; Costi, M. P.; Bolognesi, M. L. Crassiflorone Derivatives That Inhibit Trypanosoma Brucei Glyceraldehyde-3-Phosphate Dehydrogenase (TbGAPDH) and Trypanosoma Cruzi Trypanothione Reductase (TcTR) and Display Trypanocidal Activity. *Eur. J. Med. Chem.* **2017**, *141*, 138−148.
(35) Bora, K.; Sarma, M.; Kanaujia, S. P.; Dubey, V. K. Dual-Target Drugs against Leishmania Donovani for Potential Novel Therapeutics. *Sci. Rep.* **2023**, *13* (1), 18363.
(36) Lizzi, F.; Veronesi, G.; Belluti, F.; Bergamini, C.; López-Sánchez, A.; Kaiser, M.; Brun, R.; Krauth-Siegel, R. L.; Hall, D. G.; Rivas, L.; Bolognesi, M. L. Conjugation of Quinones with Natural Polyamines: Toward an Expanded Antitrypanosomatid Profile. *J. Med. Chem.* **2012**, *55* (23), 10490−10500.
(37) Macias-Silva, M.; Vazquez-Victorio, G.; Hernandez-Damian, J. Anisomycin Is a Multifunctional Drug: More than Just a Tool to Inhibit Protein Synthesis. *Curr. Chem. Biol.* **2010**, *4* (2), 124−132.
(38) Grollman, A. P. Inhibitors of Protein Biosynthesis II. MODE OF ACTION OF ANISOMYCIN. *J. Biol. Chem.* **1967**, *242* (13), 3226−3233.
(39) Hansen, J. L.; Moore, P. B.; Steitz, T. A. Structures of Five Antibiotics Bound at the Peptidyl Transferase Center of the Large Ribosomal Subunit. *J. Mol. Biol.* **2003**, *330* (5), 1061−1075.
(40) Bulkley, D.; Innis, C. A.; Blaha, G.; Steitz, T. A. Revisiting the Structures of Several Antibiotics Bound to the Bacterial Ribosome. *Proc. Natl. Acad. Sci. U.S.A.* **2010**, *107* (40), 17158−17163.
(41) Gürel, G.; Blaha, G.; Moore, P. B.; Steitz, T. A. U2504 Determines the Species Specificity of the A-Site Cleft Antibiotics: The Structures of Tiamulin, Homoharringtonine, and Bruceantin Bound to the Ribosome. *J. Mol. Biol.* **2009**, *389* (1), 146−156.
(42) Garreau De Loubresse, N.; Prokhorova, I.; Holtkamp, W.; Rodnina, M. V.; Yusupova, G.; Yusupov, M. Structural Basis for the Inhibition of the Eukaryotic Ribosome. *Nature* **2014**, *513* (7519), 517−522.
(43) Tang, Z.; Xing, F.; Chen, D.; Yu, Y.; Yu, C.; Di, J.; Liu, J. In Vivo Toxicological Evaluation of Anisomycin. *Toxicol. Lett.* **2012**, *208* (1), 1−11.
(44) Nguyen, A. M. T.; Shalev-Benami, M.; Rosa-Teijeiro, C.; Ibarra-Meneses, A. V.; Yonath, A.; Bashan, A.; Jaffe, C. L.; Olivier, M.; Fernandez-Prada, C.; Lubell, W. D. Systematic Exploration of Functional Group Relevance for Anti-Leishmanial Activity of Anisomycin. *Biomedicines* **2023**, *11* (9), 2541.
(45) Sanchez, L. M.; Knudsen, G. M.; Helbig, C.; De Muylder, G.; Mascuch, S. M.; MacKey, Z. B.; Gerwick, L.; Clayton, C.; McKerrow, J. H.; Linington, R. G. Examination of the Mode of Action of the Almiramide Family of Natural Products against the Kinetoplastid Parasite Trypanosoma brucei. *J. Nat. Prod.* **2013**, *76* (4), 630−641.
(46) Nguyen, A. M. T.; Brettell, S.; Douanne, N.; Duquette, C.; Corbeil, A.; Fajardo, E. F.; Olivier, M.; Fernandez-Prada, C.; Lubell, W. D. Influence of *N*-Methylation and Conformation on Almiramide Anti-Leishmanial Activity. *Molecules* **2021**, *26* (12), 3606.
(47) Chai, Q. Y.; Yang, Z.; Lin, H. W.; Han, B. N. Alkynyl-Containing Peptides of Marine Origin: A Review. *Mar. Drugs* **2016**, *14* (11), 216.
(48) Gogineni, V.; Hamann, M. T. Marine Natural Product Peptides with Therapeutic Potential: Chemistry, Biosynthesis, and. *Pharmacology* **2018**, *1862* (1), 81−196.
(49) Sanchez, L. M.; Lopez, D.; Vesely, B. A.; Della Togna, G.; Gerwick, W. H.; Kyle, D. E.; Linington, R. G. Almiramides A−C: Discovery and Development of a New Class of Leishmaniasis Lead Compounds. *J. Med. Chem.* **2010**, *53* (10), 4187−4197.
(50) Álvarez, G.; Varela, J.; Márquez, P.; Gabay, M.; Arias Rivas, C. E.; Cuchilla, K.; Echeverría, G. A.; Piro, O. E.; Chorilli, M.; Leal, S. M.; Escobar, P.; Serna, E.; Torres, S.; Yaluff, G.; Vera De Bilbao, N. I.; González, M.; Cerecetto, H. Optimization of Antitrypanosomatid Agents: Identification of Nonmutagenic Drug Candidates with in Vivo Activity. *J. Med. Chem.* **2014**, *57* (10), 3984−3999.

https://doi.org/10.1021/acs.jmedchem.5c01291
J. Med. Chem. 2025, 68, 20264−20282

(51) Faucher, J.-F.; Baltz, T.; Petry, K. G. Detection of an "epimastigote-like" Intracellular Stage of Trypanosoma Cruzi. *Parasitol. Res.* **1995**, *81*, 441−443.
(52) Moreno-Viguri, E.; Jiménez-Montes, C.; Martín-Escolano, R.; Santivañez-Veliz, M.; Martin-Montes, A.; Azqueta, A.; Jimenez-Lopez, M.; Zamora Ledesma, S.; Cirauqui, N.; López De Ceráin, A.; Marín, C.; Sánchez-Moreno, M.; Pérez-Silanes, S. In Vitro and in Vivo Anti-Trypanosoma Cruzi Activity of New Arylamine Mannich Base-Type Derivatives. *J. Med. Chem.* **2016**, *59* (24), 10929−10945.
(53) Rajan, K. S.; Aryal, S.; Hiregange, D. G.; Bashan, A.; Madmoni, H.; Olami, M.; Doniger, T.; Cohen-Chalamish, S.; Pescher, P.; Taoka, M.; et al. Structural and mechanistic insights into the function of Leishmania ribosome lacking a single pseudouridine modification. *Cell Rep.* **2024**, *43* (5), 114203.
(54) Rozov, A.; Khusainov, I.; El Omari, K.; et al. Importance of potassium ions for ribosome structure and function revealed by long-wavelength X-ray diffraction. *Nat. Commun.* **2019**, *10*, 2519.
(55) Paternoga, H.; Crowe-McAuliffe, C.; Bock, L. V.; Koller, T. O.; Morici, M.; Beckert, B.; Myasnikov, A. G.; Grubmüller, H.; Nováček, J.; Wilson, D. N. Structural Conservation of Antibiotic Interaction with Ribosomes. *Nat. Struct. Mol. Biol.* **2023**, *30* (9), 1380−1392.
(56) Ibarra-Meneses, A. V.; Corbeil, A.; Wagner, V.; Beaudry, F.; do Monte-Neto, R. L.; Fernandez Prada, C. Exploring direct and indirect targets of current antileishmanial drugs using a novel thermal proteomics profiling approach. *Front. Cell. Infect. Microbiol.* **2022**, *12*, 954144.
(57) De Rycker, M.; Wyllie, S.; Horn, D.; et al. Anti-trypanosomatid drug discovery: progress and challenges. *Nat. Rev. Microbiol.* **2023**, *21*, 35−50.
(58) Steitz, T. A.; Moore, P. B.; Sutcliffe, J. A.; Oyelere, A. K.; Ippolito, J. A. Ribosome Structure And Protein Synthesis Inhibitors. U.S. Patent 7,666,849 B2, February 23, 2010.
(59) Wang, S.; Dong, G.; Sheng, C. Structural Simplification: An Efficient Strategy in Lead Optimization. *Acta Pharm. Sin. B* **2019**, *9* (5), 880.
(60) Talele, T. T. Acetylene Group, Friend or Foe in Medicinal Chemistry. *J. Med. Chem.* **2020**, *63* (11), 5625−5663.
(61) Frézard, F.; Monte-Neto, R.; Reis, P. G. Antimony transport mechanisms in resistant leishmania parasites. *Biophys. Rev.* **2014**, *6* (1), 119−132.
(62) Nateghi-Rostami, M.; Tasbihi, M.; Darzi, F. Involvement of tryparedoxin peroxidase (TryP) and trypanothione reductase (TryR) in antimony unresponsive of Leishmania tropica clinical isolates of Iran. *Acta Trop.* **2022**, *230*, 106392.
(63) Prasanna, P.; Upadhyay, A. Heat Shock Proteins as the Druggable Targets in Leishmaniasis: Promises and Perils. *Infect. Immun.* **2021**, *89* (2), No. e0055920.
(64) Vergnes, B.; Gourbal, B.; Girard, I.; Sundar, S.; Drummelsmith, J.; Ouellette, M. A. Proteomics Screen Implicates HSP83 and a Small Kinetoplastid Calpain-Related Protein in Drug Resistance in Leishmania Donovani Clinical Field Isolates by Modulating Drug-Induced Programmed Cell Death. *Mol. Cell. Proteomics* **2007**, *6* (1), 88−101.
(65) Padmanabhan, P. K.; Samant, M.; Cloutier, S.; Simard, M. J.; Papadopoulou, B. Apoptosis-like Programmed Cell Death Induces Antisense Ribosomal RNA (rRNA) Fragmentation and rRNA Degradation in Leishmania. *Cell Death Differ.* **2012**, *19*, 1972−1982.
(66) De Muylder, G.; Ang, K. K.; Chen, S.; Arkin, M. R.; Engel, J. C.; McKerrow, J. H. A Screen against *Leishmania* Intracellular Amastigotes: Comparison to a Promastigote Screen and Identification of a Host Cell-Specific Hit. *PLoS Neglected Trop. Dis.* **2011**, *5*, No. e1253.
(67) Bhattacharya, A.; Corbeil, A.; do Monte-Neto, R. L.; Fernandez-Prada, C. Of Drugs and Trypanosomatids: New Tools and Knowledge to Reduce Bottlenecks in Drug Discovery. *Genes* **2020**, *11* (7), 722.
(68) Hu, C.; Li, G.; Mu, Y.; Wu, W.; Cao, B.; Wang, Z.; Yu, H.; Guan, P.; Han, L.; Li, L.; Huang, X. Discovery of Anti-TNBC Agents Targeting PTP1B: Total Synthesis, Structure-Activity Relationship, In Vitro and In Vivo Investigations of Jamunones. *J. Med. Chem.* **2021**, *64* (9), 6008−6020.
(69) Ojima, D.; Yasui, A.; Tohyama, K.; Tokuzumi, K.; Toriihara, E.; Ito, K.; Iwasaki, A.; Tomura, T.; Ojika, M.; Suenaga, K. Total Synthesis of Miuraenamides A and D. *J. Org. Chem.* **2016**, *81* (20), 9886−9894.
(70) Ideue, E.; Toma, T.; Shimokawa, J.; Fukuyama, T. Convenient Synthesis of α-Diazoacetates from α-Bromoacetates and *N,N′*-Ditosylhydrazine: Preparation of Benzyl Diazoacetate. *Org. Synth.* **2012**, *89*, 501−509.
(71) Still, W. C.; Kahn, M.; Mitra, A. Rapid Chromatographic Technique for Preparative Separations with Moderate Resolution. *J. Org. Chem.* **1978**, *43*, 2923−2925.
(72) Leprohon, P.; Legare, D.; Raymond, F.; Madore, E.; Hardiman, G.; Corbeil, J.; Ouellette, M. Gene expression modulation is associated with gene amplification, supernumerary chromosomes and chromosome loss in antimony-resistant Leishmania infantum. *Nucleic Acids Res.* **2009**, *37*, 1387−1399.
(73) Brotherton, M. C.; Bourassa, S.; Leprohon, P.; Legare, D.; Poirier, G. G.; Droit, A.; Ouellette, M. Proteomic and genomic analyses of antimony resistant Leishmania infantum mutant. *PLoS One* **2013**, *8*, No. e81899.
(74) Brotherton, M. C.; Bourassa, S.; Legare, D.; Poirier, G. G.; Droit, A.; Ouellette, M. Quantitative proteomic analysis of amphotericin B resistance in Leishmania infantum. *Int. J. Parasitol.: Drugs Drug Resist.* **2014**, *4* (2), 126−132.
(75) Fernandez-Prada, C.; Vincent, I. M.; Brotherton, M. C.; Roberts, M.; Roy, G.; Rivas, L.; Leprohon, P.; Smith, T. K.; Ouellette, M. Different Mutations in a P-type ATPase Transporter in Leishmania Parasites are Associated with Cross-resistance to Two Leading Drugs by Distinct Mechanisms. *PLoS Neglected Trop. Dis.* **2016**, *10*, No. e0005171.
(76) Zivanov, J.; Nakane, T.; Forsberg, B. O.; Kimanius, D.; Hagen, W. J.; Lindahl, E.; Scheres, S. H. New tools for automated high-resolution cryo-EM structure determination in RELION-3. *Elife* **2018**, *7*, No. e42166.
(77) Zheng, S.; Palovcak, E.; Armache, J. P.; et al. MotionCor2: anisotropic correction of beam-induced motion for improved cryo-electron microscopy. *Nat. Methods* **2017**, *14*, 331−332.
(78) Mindell, J. A.; Grigorieff, N. Accurate determination of local defocus and specimen tilt in electron microscopy. *J. Struct. Biol.* **2003**, *142*, 334−347.
(79) Nakane, T.; Kimanius, D.; Lindahl, E.; Scheres, S. H. Characterisation of molecular motions in cryo-EM single-particle data by multi-body refinement in RELION. *Elife* **2018**, *7*, No. e36861.
(80) Emsley, P.; Lohkamp, B.; Scott, W. G.; Cowtan, K. Features and development of Coot. *Acta Crystallogr., Sect. D: Biol. Crystallogr.* **2010**, *66* (4), 486−501.
(81) Pettersen, E. F.; Goddard, T. D.; Huang, C. C.; Meng, E. C.; Couch, G. S.; Croll, T. I.; Morris, J. H.; Ferrin, T. E. UCSF ChimeraX: Structure visualization for researchers, educators, and developers. *Protein Sci.* **2021**, *30* (1), 70−82.
(82) Auffinger, P.; Ennifar, E.; D'Ascenzo, L. Deflating the RNA Mg2+ bubble. Stereochemistry to the rescue. *RNA* **2021**, *27* (3), 243−252.
(83) Afonine, P. V.; Poon, B. K.; Read, R. J.; Sobolev, O. V.; Terwilliger, T. C.; Urzhumtsev, A.; Adams, P. D. Real-space refinement in PHENIX for cryo-EM and crystallography. *Acta Crystallogr., Sect. D: Struct. Biol.* **2018**, *74* (6), 531−544.
(84) Williams, C. J.; Headd, J. J.; Moriarty, N. W.; Prisant, M. G.; Videau, L. L.; Deis, L. N.; Verma, V.; Keedy, D. A.; Hintze, B. J.; Chen, V. B.; Jain, S.; Lewis, S. M.; ArendallSnoeyinkAdams, W. B. J. P. D.; Lovell, S. C.; Richardson, J. S.; Richardson, D. C.; Richardson, J. S.; Richardson, D. C. MolProbity: More and better reference data for improved all-atom structure validation. *Protein Sci.* **2018**, *27* (1), 293−315.
(85) Laskowski, R. A.; Swindells, M. B. LigPlot+: multiple ligand-protein interaction diagrams for drug discovery. *J. Chem. Inf. Model.* **2011**, *51*, 2778−2786.

https://doi.org/10.1021/acs.jmedchem.5c01291
J. Med. Chem. 2025, 68, 20264−20282